HHS Public Access

Author manuscript

J Opt. Author manuscript; available in PMC 2020 February 12.

Published in final edited form as:

J Opt. 2019 October ; 21(10): . doi:10.1088/2040-8986/ab3b1a.

Listening to tissues with new light: recent technological advances in photoacoustic imaging

Tri Vu[1], **Daniel Razansky**[2,3], **Junjie Yao**[1]

[1]Photoacoustic Imaging Lab, Department of Biomedical Engineering, Duke University, Durham, NC, USA [2]Faculty of Medicine and Institute of Pharmacology and Toxicology, University of Zurich, Switzerland [3]Institute for Biomedical Engineering and Department of Information Technology and Electrical Engineering, ETH Zurich, Switzerland

Abstract

Photoacoustic tomography (PAT), or optoacoustic tomography, has achieved remarkable progress in the past decade, benefiting from the joint developments in optics, acoustics, chemistry, computing and mathematics. Unlike pure optical or ultrasound imaging, PAT can provide unique optical absorption contrast as well as widely scalable spatial resolution, penetration depth and imaging speed. Moreover, PAT has inherent sensitivity to tissue's functional, molecular, and metabolic state. With these merits, PAT has been applied in a wide range of life science disciplines, and has enabled biomedical research unattainable by other imaging methods. This Review article aims at introducing state-of-the-art PAT technologies and their representative applications. The focus is on recent technological breakthroughs in structural, functional, molecular PAT, including super-resolution imaging, real-time small-animal whole-body imaging, and high-sensitivity functional/molecular imaging. We also discuss the remaining challenges in PAT and envisioned opportunities.

Keywords

photoacoustic tomography; optoacoustic tomography; photoacoustic microscopy; photoacoustic computed tomography; super-resolution imaging; molecular imaging; functional imaging

1. Introduction

Photoacoustic (PA) imaging (or optoacoustic imaging) exploits a physical phenomenon that uses light (*i.e.* "photo-") to generate sound (*i.e.* "-acoustic") through thermal expansion induced by absorption of the photon energy. In fact, the same effect can be induced by any electromagnetic waves, including visible and near-infrared light, radio-frequency waves, x-ray photons, and even γ rays. Even though the original discovery of the *photophonic* phenomenon by Alexander Graham Bell dates back to 1880 (4, 5), it was not until the early 1990s that the effect was initially applied in biomedical imaging, later known as photoacoustic tomography (PAT, or optoacoustic tomography), in which visible and near-

daniel.razansky@uzh.ch, junjie.yao@duke.edu.

infrared laser light is most commonly used as the excitation source. Physically combining the optical excitation and ultrasonic detection, PAT offers rich optical contrast at depths far beyond those achieved by conventional high-resolution optical microscopy. Enabled by the new developments in laser, ultrasound and computer science technologies in the early 2000s, PAT has advanced quickly from proof-of-concept lab technologies to popular biomedical research tools.

Two major categories of PAT technologies exist: photoacoustic microscopy (PAM) and photoacoustic computed tomography (PACT). Generally, PAM is often used for high-resolution imaging within a depth of several millimeters, while PACT is mostly utilized for volumetric imaging with a larger penetration depth beyond one centimeter at the expense of inferior spatial resolution. One of the most recent advances in PAM is super-resolution imaging, enabled by non-linear mechanisms, such as two-photon absorption (8–10), absorption saturation (11–15), thermal relaxation (12, 16, 17), photothermal bleaching (18, 19) and reversible photoswitching (6, 20, 21). Meanwhile, PACT has made significant progress in attaining three-dimensional (3D) (22–24), real-time (25, 26), and whole-body small-animal imaging (27, 28) performance. The rapid technical evolution of PAT has enabled a wide range of applications in both pre-clinical research and clinical translation. For example, high-resolution PAM is exploited in single cell imaging, including flow oximetry (29), flow cytometry (30, 31) and tissue engineering (32, 33). PACT with superior penetration depths is extensively applied in functional small-animal studies such as mapping neural-activity mapping (34), measuring blood oxygenation (35, 36) and monitoring cardiac functions (37). Moreover, PAT has been increasingly used in oncology, particularly for cancer screening (38–41).

Recent Review articles have focused on different aspects of PAT. For example, Li *et al.* have presented a report on PAT of blood oxygenation (13). Yao *et al.* have provided an overview of the recent process in PA molecular imaging (42). Other examples include Reviews on single cell PAM (43), PA blood flow imaging (44), PAT of genetically encoded reporters (45), molecular contrast agents for PAT (46, 47), PA spectroscopy (48, 49), and ultrasonic transducers in PAT (50). In this concise Review, we focus on recent technical advances in PAT and their corresponding applications. We discuss the outstanding technical challenges in PAT and envision future technological and application-related breakthroughs, such as single molecule detection and deep-human-brain functional imaging. Last but not least, we also provide perspectives on promising clinical translations in PAT, such as early detection of cancer and cardiovascular disease and surgical guidance.

2. Overview of PAT

In this section, we introduce the technical basics of PAT, including the imaging principles as well as the multi-scale and multi-contrast imaging capabilities. Readers are referred to more comprehensive Review articles on each of the sub-sections (14, 47, 51).

2.1 Basic Principles

The imaging process of PAT includes two main steps: optical excitation and ultrasonic detection. In the first step, short laser pulses are delivered to illuminate biological tissues. As

photons propagate through tissue, biomolecules absorb some of the optical energy that is partially or fully converted into thermal energy, resulting in thermal expansion and local pressure rise. The pressure rise propagates in the tissue as ultrasonic waves. This process is depicted in Fig. 1. The optical wavelength, pulse energy, pulse width, and pulse repetition rate are optimized to maximize the PA signal generation. In the second step, the laser-induced ultrasonic waves are detected at the tissue surface by a single ultrasonic transducer or an array. The received ultrasonic signals are then used to reconstruct the original optical energy deposition inside the tissue using different inversion schemes. Therefore, the rich optical absorption contrast of biological tissues is responsible for the excellent functional, molecular, and metabolic imaging capacities of PAT. On the other hand, the generated ultrasonic waves can propagate in the tissue with much less attenuation and scattering than the light photons, thus PAT can provide acoustically-determined spatial resolution at depths far beyond that achieved by optical microscopy (52). The hybrid combination of light and ultrasound enables PAT to achieve highly scalable imaging performance with consistent and diverse contrast mechanism.

PAT can be grouped into two major implementations based on the image acquisition strategy. PAM typically relies on a direct image acquisition by raster-scanning focused ultrasound transducers in order to form images (14). PAM can be further classified into optical-resolution PAM (OR-PAM) and acoustic-resolution PAM (AR-PAM). While OR-PAM uses tight optical focusing to provide the optically-determined lateral resolution within the optical diffusion limit (~1 mm in soft tissue), AR-PAM uses weakly focused light and provides acoustically-determined spatial resolution at depths up to several millimeters (14). PACT typically employs wide-field light illumination and multi-channel unfocused ultrasound detection, and depends on inverse image reconstruction methods, such as delay-and-sum, back-projection, time-reversal or model-based algorithms, to form the final images (14, 53). PACT typically operates at lower ultrasound frequencies (1–10 MHz) than PAM (20–75 MHz), providing greater imaging depths (> 1 cm) but lower spatial resolutions.

2.2 Multi-Scale PAT

PAT is capable of high-resolution imaging at different scales, with the trade-off between the spatial resolution and penetration depth. Across the scales, PAT maintains a high depth-to-resolution-ratio (DRR) of more than 200, qualifying it as a high-resolution imaging modality. For example, with sub-micrometer resolution and a penetration depth of < 1 mm, OR-PAM can image single cells and sub-cellular structures such as red blood cells (31, 54), osteoblast (55), mitochondria (2), and neutrophils (56). With sub-millimeter resolution and a penetration depth of >3 mm, AR-PAM can visualize subcutaneous blood vessels in the human palm (57) and deep-brain vasculature in small animals (58). Further, PACT can achieve a penetration of several centimeters for human and whole-body small animal imaging (34, 39, 59, 60). Overall, PAT's high scalability can enable biomedical studies of the same biological process on cells, small animals, and even humans with consistent contrast mechanisms (61).

2.3 Multi-Contrast PAT

PAT's multi-contrast imaging capability originates from the physical process making the amplitude of the PA signal to be proportional to the product of optical absorption coefficient of the imaged target and the local optical fluence. In other words, PAT has a 100% sensitivity to variations in the optical absorption contrast. Different molecules typically have unique absorption spectra. Therefore, various endogenous and exogenous labels can be used in PAT to target specific functional and molecular processes. Endogenous labels have several major advantages: (1) no toxicity, (2) unperturbed biology, (3) abundance, and (4) avoidance of regulatory approval. Endogenous molecules such as hemoglobin, melanin, lipid, water, and collagen are imaged in PAT for estimation of blood oxygenation (62–64), imaging-guided photothermal ablation of melanoma (65), cancer screening (41), and intravascular imaging of coronary atherosclerosis (66, 67). On the other hand, similar to fluorescence imaging, the utilization of rich exogenous contrast agents has tremendously broadened PAT's applications that require high molecular sensitivity and specificity, particularly in cancer diagnosis and treatment. Exogenous contrast agents have two advantages over endogenous ones (68, 69): (1) optimization for greater detection sensitivity and (2) conjugation with targeting molecules (e.g., antibodies) to selectively bind to receptors for molecular imaging. For example, nanoparticles have been extensively used for monitoring photothermal therapy and guiding lymph node biopsy (70–78). Dyed microbubbles have been used for dual-modality ultrasound imaging and PAT in nanoparticle delivery and tumor imaging (79–81). All in all, PAT's multi-contrast imaging capability can provide optical-absorption-based functional and molecular information, which is, in fact, the major advantage of PAT over pure ultrasound imaging.

3. Recent Advances in PAT technologies

Here, we summarize the most exciting advances in PAT technologies that have overcome the limits in structural, functional, molecular imaging, and other system attributes, including super-resolution PAT, real-time small-animal whole-body PAT, remote-sensing PAT, high-sensitivity functional/molecular PAT, and machine-learning enhanced PAT.

3.1. Structural PAT

In this section, we discuss the new techniques that aim at improving the capability of PAT to image structures with high resolution, high speed and large penetration depth. These techniques include recent breakthroughs in super-resolution and real-time imaging of biological structures at both microscopic and macroscopic levels.

3.1.1 Super-Resolution PAT (SR-PAT)—In conventional OR-PAM, the spatial resolutions are generally limited by the optical diffraction in the lateral direction and the acoustic detection bandwidth in the axial direction. One approach to overcome the optical diffraction in OR-PAM is to explore nonlinear signal generation mechanisms, such as the **two-photon absorption**, which has long been used in two-photon microscopy deeper penetration and reduced photo-bleaching (82, 83). In contrast to two-photon microscopy, the major technical challenge in two-photon PAM is the separation of nonlinear two-photon signals from their linear single-photon counterparts. One solution by Yamaoka *et al.* uses

time-gated detection and frequency filtering (10, 84–87), while another study by Lee *et al.* employs a loss modulation technique. Two-photon PAM has provided a lateral and axial resolution of 0.51 μm and 2.41 μm, respectively (Fig. 2(a)) (1). The major advantage of two-photon PAM over single-photon PAM is the much improved axial resolution due to the optical sectioning. However, one clear drawback of two-photon absorption is the significantly reduced PA signal strength due to the low two-photon absorption coefficient, resulting in diminished imaging depth.

Other nonlinear mechanisms have also been explored to achieve sub-diffraction resolutions in PAM, including **transient optical absorption** (88, 89), **optical absorption saturation** (2, 11), and **thermal relaxation** (7, 90). All these methods share the same goal–nonlinear PA signal generation, and can be applied to any samples. The transient optical absorption based method modulates the number of ground-state electrons by using a strong excitation laser beam. Similarly, the optical absorption saturation-based method exploits the dependence of ground-state electrons on the excitation optical fluence (Fig. 2(b)) (2, 11). The thermal relaxation-based method utilizes the dependence of Grüneisen parameter on the optical fluence (7). The Grüneisen parameter reflects the conversion efficiency from the optical to acoustic energy in the PA signal generation. The thermal-relaxation-based PAM has improved the lateral resolution from 0.65 μm to 0.41 μm and the axial resolution from 45 μm to 2.3 μm (Fig. 2(c)) (7, 90). Photothermal bleaching and reversible photoswitching are two nonlinear mechanisms that permanently or temporally modulate the sample's optical absorption coefficient. Both methods rely on the dependence of the absorption coefficient on the local optical fluence. The photothermal bleaching based method measures the difference in PA signals before and after bleaching to improve the spatial resolution (Fig. 2(d)) (7, 91, 92). In the reversible photoswitching based method, light-absorbing proteins such as BphP1, can be switched between two absorbing states (6), (92). The differential PA signals between the two states have nonlinear dependence on the optical fluence, which may lead to a sub-diffraction spatial resolution in the 140 nm range (Fig. 2(d))(6, 93). The photobleaching method, however, may cause damage to the imaged sample whereas photoswitching employs switchable contrast agents, thus restricting broad applicability.

To achieve super-resolution in AR-PAM and PACT, in which the spatial resolution is largely determined by the acoustic diffraction limit, researchers have so far exploited **temporal fluctuations**, **wavefront shaping**, and **sparse absorber localization** technique. For example, recent studies have reported resolution enhancement of 1.4 fold by using the speckle-illumination-induced signal fluctuations, and resolution enhancement of $\sqrt{n}$ fold (with n-th order of cumulant images) by using flow-induced signal fluctuations (94, 95). Using wavefront shaping, a six-fold resolution improvement has been shown in a scattering medium (96). By extracting and superimposing central positions of flowing targets over multiple image frames, localization-based PACT is able to achieve sub-diffraction spatial resolution and reduce the limited-view artifacts (97). All of the above super-resolution methods have great potential to enable deeper photoacoustic imaging with superior resolution over conventional PAT, and allow functional and molecular imaging at depths of several centimeters, far beyond the optical diffusion limit. However, superior spatial resolution usually comes at a cost of diminished temporal resolution, where multiple frames

have been combined in order to form a single super-resolution image. As a consequence, these methods may not be capable of capturing rapid biological dynamics.

3.1.2 Dynamic PACT—PAT is well suited for deep-tissue dynamic imaging on small animal models, taking advantage of the near-infrared optical excitation, low-frequency ultrasound detection, and parallel data acquisition. The recent advances in PACT technologies include 3D real-time multi-spectral imaging, whole-body small-animal imaging. It was initially challenging for PACT to achieve real-time image rendering, due to a large number of simultaneously recorded time-resolved transducer channels and the heavy computational workload. Benefiting from the recent progress in **graphics processing unit** (GPU) based computation, the image reconstruction in PACT has been significantly accelerated to attain high-speed volumetric imaging in humans (98, 99) and mice (100). Moreover, **compressed-sensing** (CS) based image reconstruction has been applied in real-time PACT with spatial under-sampling (101–106). Ozbek *et al.* have developed a high-speed PACT system that combines CS with GPU-enhanced image reconstruction, attaining a 3D frame rate of 1.6 kHz (107), more than 10 times faster than the previously reported PACT imaging speed. A principal component analysis based method has also been developed to accelerate PACT's image reconstruction (108, 109). The downside of the CS-based methods is the reduced performance when imaging densely distributed targets.

Important progress has also been recently achieved in whole-body small-animal imaging with PACT. Traditionally, PACT systems using linear arrays and other acquisition geometries with limited tomographic coverage and/or multiplexed data acquisition have suffered from limited-view artifacts, spatial under-sampling, and breathing motion artifacts, which collectively result in low image quality (27, 110–113). A recent work by Li *et al.* has reported **single-impulse panoramic PACT** (SIP-PACT), as shown in Fig. 3(a), which uses a 512-channel ring-shaped ultrasound transducer array coupled with a 512-channel data acquisition system. There is no data multiplexing needed, so each laser pulse can provide a complete 2D image of the mouse's cross section. SIP-PACT has largely addressed the aforementioned issues and achieved a 2D frame rate of 50 Hz, in-plane spatial resolution of 125 μm, and much-reduced limited-view and breathing-motion artifacts (114, 115). With superior imaging performance, SIP-PACT has been used for tracking circulating tumor cells and quantifying whole-body oxygenation (116). Most recently, Merčep *et al.* have reported on a new implementation of a full-ring array geometry for high-quality hybrid transmission-reflection optoacoustic ultrasound (TROPUS) computed tomography of small animals (117). Yet, SIP-PACT needs translational scanning along the elevational direction for volumetric imaging. Moreover, it suffers from poor elevational resolution, resulting in volumetric images exhibiting highly anisotropic resolution. Another important recent work in small-animal whole-body PACT is the **spiral volumetric optoacoustic tomography** (SVOT), developed by the Razansky group (118, 119). The system schematics is illustrated in Fig. 3(b). Using a semi-spherical ultrasound transducer array, SVOT is capable of real-time multi-spectral imaging within a volume of 1 cm^3 (119). At each wavelength, SVOT can provide a maximum 3D frame rate of 100 Hz, with an isotropic in-plane resolution of 250 μm (119). SVOT's multi-spectral imaging capability was demonstrated by real-time mapping of exogenous contrast agent distribution (119). Both SIP-PACT and SVOT have

shown great promise for biomedical applications at the whole-body scale, such as monitoring cancer progress, tracking drug delivery, and evaluating treatment responses.

Besides the conventional acoustic detection using piezoelectric transducers, novel **all-optical PAT** systems employing optical detection of acoustic waves have become an important research topic (120). All-optical acoustic detectors can provide a better detection sensitivity per unit area and a wider detection bandwidth than piezoelectric transducers, both of which are highly desired in PAT to improve the imaging depth and spatial resolution. For example, Fabry-Perot sensors have been developed in Paul Beard's group, in which the PA pressure waves are detected by optically reading the modulation of the sensor's optical thickness (121). The Fabry-Perot-based PACT shows superior image quality over traditional PACT with piezoelectric transducers, mainly due to the broader detection bandwidth extending into the low-frequency range and smaller effective detector size as defined by the size of the probing beam (121). More recent advances include using multiple probing beams to reduce image acquisition time (122–124) and plano-concave sensor to improve the detection sensitivity (125). We will discuss the all-optical PAT with remote sensing in Section 3.4.1.

In addition to the imaging speed, recent advances in PACT also include compact laser systems (23), improved SNR and elevational resolution (126, 127), low-cost light sources (128–132), and high-speed multispectral excitation (26, 112, 133, 134). Together, these advances have greatly enhanced PACT's imaging performance, especially in pre-clinical applications, and enabled a variety of biomedical studies by simultaneously providing large field of view, extended imaging depth, high imaging speed, functional and molecular sensitivity.

3.2 Functional PAT

Fundamentally, PAT's functional imaging capability originates from its unique sensitivity to optical absorption contrast. PAT has been previously used for measuring blood oxygenation, blood flow, temperature, and oxygen metabolism, as well as monitoring the tumor microenvironment (*e.g.*, pH), tracking targeted molecular agents, and enumerating the circulating tumor cells. Nevertheless, one major challenge in functional PAT is the quantification accuracy of the physiological parameters in deep tissues beyond the optical diffusion limit, mainly due to the unknown tissue optical properties and the wavelength-dependent optical attenuation (*i.e.*, spectral coloring). To address these issues, a number of methods have been developed to improve the absolute quantification and detection sensitivity. A number of representative examples are described below to highlight this highly active research topic.

Firstly, for blood flow measurement in deep tissue, a family of thermally-encoded methods have been developed. In general, the thermally-encoded flow methods take advantage of PAT's sensitivity to the blood temperature. By optically or acoustically increasing the local blood volume's temperature, PAT can track the motions of the heated blood volume and quantify the flow speed. In particular, **ultrasound-encoded photoacoustic flowgraphy** (UE-PAF) has demonstrated superior performance over Doppler-based PA flow measurement (17). UE-PAF, as shown in Fig. 4(a), uses a single-element focused ultrasonic transducer to periodically elevate the blood temperature within the acoustic focus, while the

PACT system using a ring-shaped transducer array acquires the images of the heated blood and tracks its motion (17, 135, 136). Since focused ultrasound waves can penetrate several centimeters into the tissue and induce rapid temperature rise, UE-PAF has successfully measured blood flow in deep mouse brain. Using hemoglobin as the endogenous contrast, the thermally-encoded methods are capable of measuring slow blood flow on the level of 0.1 mm/s (17, 137). More recent works using lasers for optical heating and PA imaging have simplified the system configuration and improved the spatial resolution, at the cost of imaging depth (137, 138).

Secondly, for oxygenation measurement, researchers have been investigating **PA lifetime imaging** (PALI), which relies on the oxygen-dependent excited-state lifetime of the sensor and is not prone to the tissue's wavelength-dependent optical attenuation. PALI can potentially be applied for imaging guidance or treatment evaluation in photodynamic therapy and radiotherapy of cancers (139). Recent works have demonstrated PALI using methylene blue (127, 140, 141), and achieved oxygenation mapping at 15 mm depth with sub-millimeter spatial resolution (127, 139, 142). Another solution to the issue of unknown optical fluence at depths was recently demonstrated in **eigenspectral multispectral optoacoustic tomography** (eMSOT) (143, 144). eMSOT assumes that only a small number of fundamental spectra (four base spectra and three fluence eigenspectra) exist in biological tissues, and any fluence spectrum can be predicted by combining these spectra and thus the blood oxygenation can be computed (144). eMSOT has demonstrated superior performance in deep tissues *in vivo*, illustrated in Fig. 4(b), and reduced mean sO_2 measurement error from 35% by the traditional linear unmixing method to 4% (144).

Thirdly, great efforts have been spent on noninvasive measurement of blood glucose level for diabetic patients. Although measuring blood glucose level has been long sought after as a highly promising PA application, the low detection specificity has prevented its adoption in clinically relevant settings. Namita *et al.* have recently reported that the glucose concentration in either water or blood can be quantified from the PA signals acquired at 1120 nm (145). Sim *et al.* have demonstrated that it is possible to measure the glucose level in skin's secretion products, using PA spectroscopy with a mid-infrared wavelength range of 8–10.5 μm (146). With relatively simple control of the skin conditions, the PA spectroscopy method has great potential for clinical translation (146). Other studies on PA glucose monitoring include linear calibration (147, 148), Helmholtz resonance cell (149) and multi-modal broadband dielectric spectroscopy (150). All these endeavors have contributed to the growing knowledge of optimizing PAT's configurations and data analysis for accurate glucose measurement.

Last but not least, PAT can measure temperature, taking advantage of the Grüneisen parameter's temperature dependence. Early studies employed this dependence to measure relative temperatures in single cells (151) and deep tissues (152, 153). Latest works have developed portable blood temperature monitoring (154) and dual-wavelength thermometry to reduce random errors (155). Absolute temperatures in deep tissues have been measured by exploring the dual temperature dependence of the Grüneisen parameter and the speed of sound (156), or by incorporating a multi-illumination scheme (157). Real-time volumetric PA monitoring of temperature distribution during photothermal therapy has further been

demonstrated (5). Complementary to ultrasound and MRI thermometry (153), PA thermometry has a great potential to be incorporated with cancer thermal treatments to precisely control the temperature for maximized treatment effect and minimized thermal damage (158).

3.3 Molecular PAT

In addition to measuring various functional parameters, significant advances have been made in PA molecular imaging, especially for its quantification accuracy and detection sensitivity in deep tissues. Readers are referred to the recent Review article on the state-of-the-art molecular PAT technologies (42). One major challenge in molecular PAT is the relatively low detection sensitivity of genetically encoded probes, which are typically expressed at a low concentration level and can be easily shadowed by the strong background signals from blood. Recent methods based on compensating for the optical fluence, enhancing non-radiative relaxation, or extracting the signal's temporal changes have been developed to improve the quantification accuracy in molecular PAT. These novel engineering strategies have been individually or concurrently implemented with novel PAT-specific molecular probes, aiming to improve the detection sensitivity. In addition to improving PAT's detection sensitivity, another important research topic is integrating PAT with other imaging modalities with superior localizing capability or complementary contrast mechanism. In this section, we will discuss in details about new molecular PAT technologies, representative molecular probes, as well as their applications.

3.3.1. Enhanced molecular PAT based on modulation of optical properties—

Activatable or photoswitchable molecular probes with NIR absorption, such as bacterial phytochrome and semiconducting polymer nanoparticles, have been optimized or engineered as PA contrast agents. By optically or chemically modulating the optical absorption of these molecular probes, one can suppress the background signals through ratiometric or differential measurements. The enhanced detection sensitivity has enabled the studies of reactive oxygen species, pH–vital chemical mediator, cancer metastasis, and cardiovascular diseases (159–161). Other activatable probes, including nitric oxide, hyaluronic acid nanoparticles and CuS nanodots, have also been explored for molecular PAT in mouse tumor models (160, 162–167).

Besides using activatable or photoswitchable probes, researchers have recently demonstrated the use of **intraparticle engineering** and **self-quenched probes** to enhance photoacoustic signals (168, 169). In intraparticle engineering, a secondary optical dopant is incorporated into the semiconducting polymer nanoparticle to quench its fluorescence and enhance nonradiative relaxation (168, 169). However, this method suffers from the potential leakage of the dopant from the nanoparticle (168). The self-quenched approach incorporates an electron-deficient structure unit into the backbone of the semiconducting polymers to enhance the heat generation and thus PA signals (168).

3.3.2. Enhanced molecular PAT based on temporal modulations of the PA signals—

Alternatively, **magnetomotive PAT** has demonstrated improved detection sensitivity. While aforementioned techniques in Section 3.3.1 modulate the optical

properties of the molecular probes, magnetomotive PAT relies on the physical displacement of the probes driven by an oscillating magnetic field. By “poking” the magnetic nanoparticles using magnetic force, PAT can suppress the background signals from non-magnetic biomolecules, and thus improve the detection sensitivity (170). Magnetomotive PAT has been demonstrated on gold-shelled or polymer-shelled magnetic nanoparticles (171, 172). Moreover, calcium-sensitive indicators have also been used by PAT to study neuron activities. These calcium indicators include arsenazo III (173), GCaMP (174), CaSPA550 (175), NIR metallochromic compounds (176), and acoustogenic probes for copper(II) (177). However, unlike two-photon microscopy, PAT cannot yet visualize individual neurons in the mouse brain, limited by the spatial resolution in deep tissues (173).

3.3.3. Molecular PAT with multi-modal contrast—PAT has been integrated with other imaging techniques, such as magnetic resonance imaging (MRI), Raman imaging and positron emission tomography (PET). MRI, while providing accurate localization of lesions, has difficulty to provide sufficient molecular sensitivity. This limitation of MRI can be complemented by PAT. Dual-modal contrast agents have been developed for PAT and MRI, such as lipid-micelles incorporated with semiconducting polymer dots, a photosensitizer, and PEGylated polypyrrole nanoparticle (178, 179), as well as Gadolinium(III)-gold nanorods for macrophage detection in atherosclerotic inflammation (180). Moreover, PAT has been incorporated with Raman imaging and PET for enhanced molecular performance. Kircher *et al.* integrated surface-enhanced Raman scattering (SERS) with PAT/MRI for tumor margin detection (181), in which Gold silica–based SERS nanoparticles coated with Gd3+ were used to visualize the brain tumor with high spatial resolution (181). PET was also integrated with PAT/MRI for imaging reporter-gene products with high sensitivity (182).

3.4 Other Technical Advances in PAT

Here, we also introduce other PAT advances that focus on addressing the technical obstacles from various perspectives, such as the need for coupling medium, reconstruction artifacts, and the integration with other imaging modalities.

3.4.1 Non-contact (remote-sensing) PAT—In PAT, the need for a coupling medium (*e.g.*, water, ultrasound gel) or direct contact with the targets has been considered a technical disadvantage in comparison with other pure optical imaging modalities. The need for coupling substantially increases the complexity of the system configuration and experimental procedures. Therefore, new methods have been reported on non-contact PAT that does not need any coupling during the imaging process. These non-contact PAT methods mostly utilize optical sensing of the acoustic signals, for example, by detecting the displacement of the sample surface induced by pressure waves. The pressure-induced surface displacement can be captured by **optical interferometers**. The recorded optical signals are then used for the image reconstruction. A number of optical interferometer techniques have been explored in non-contact PAT, including Mach-Zehner interferometer (183), Fabry-Perot interferometer (184, 185), Michelson interferometer (186), photoreactive-crystal two-wave mixing (187, 188), and speckle-tracking-based interferometry (189, 190). Moreover, recent studies have focused on compact detecting systems using fiber-based

interferometers, which have further reduced the system footprint and may enable endoscopic applications (191–193). This fiber-based approach has been expanded to a line-detector setup with multiple fibers in **photoacoustic projection imaging**, which is similar to the X-ray computed tomography and capable of all-optical volumetric imaging (194, 195). Overall, the advances in non-contact PAT have the potential to overcome the traditional barriers for clinical applications such as thyroid cancer detection, burn evaluation, and brain surgery guidance (191). Recently, a non-interferometry-based optical sensing method has been developed for detecting the PA pressures through the changes in the tissue's refractive index (196). This method is promising for integrating with other optical imaging modalities, such as OCT for ophthalmological applications (196).

3.4.2 Machine Learning in PAT—The PAT community is also closely following the current computational revolution in machine learning. In the past several years, different machine learning methods have been explored to reduce the reconstruction artifacts in PACT images, without the need for increasing the acoustic detection aperture or spatial sampling frequency. For example, **U-Net**, an encoder-decoder-based convolutional neural network originally developed for image segmentation, has been adapted in PACT for direct image reconstruction or correction of the delay-and-sum method (22, 197, 198). The machine learning methods have shown promising performance in eliminating reconstruction artefacts with simulation data, with an l_2–reconstruction error of 1% (198). Reverberation artifacts can also be reduced by training the network to identify the signal reflection patterns (199, 200). A recent study by Antholzer *et al.* has been successful in correcting the frequency-limited and angle-limited ultrasound detection for real-time projection imaging (201–203). It integrates U-Net with **dynamic aperture-length correction** (applying learnable weights to reconstruction grid points) (202, 203). Another application of machine learning in PAT is to improve the quantification accuracy without knowing the prior information of the tissue's optical properties. For example, Kirchner *et al.* have implemented a context-encoded fluence distribution map with random forest regression to estimate blood oxygenation on simulation data (204). Another study, which also utilizes U-Net with extra skip connections, takes raw radiofrequency data at different wavelengths to reconstruct blood oxygenation and molecular probe concentrations (205). All in all, machine learning, although still a relatively new concept in PAT, has been providing possible solutions for many long-standing technical challenges, mostly for artifact elimination, without complicating the system setup or increasing the cost. Machine learning in PAT may also help automatic diagnosis and staging of diseases, such as breast cancer. However, a typical challenge that machine learning methods face is the lack of training data with ground truth acquired in experimental or clinical settings. Simulation is still the primary source of data generation, which does not provide necessary variation to effectively train the learning models. Data augmentation on simulation data can be used to increase the robustness of network training.

3.4.3. Hybrid photoacoustic-ultrasound (PAUS) imaging—The high complementarity of pulse-echo ultrasonography (US) and PAT has also prompted the development of combined approaches that utilize the same transducer array for visualizing both contrasts. Yet, an efficient integration is not straightforward as it implies accounting for the fundamentally different excitation and image formation strategies of those modalities.

Initially, hybrid imaging was achieved by adding fiber-guided light irradiation next to the conventional US linear array probe (206). Although this acquisition geometry attains good performance in sensing back-scattered ultrasonic waves, it is proved to be inefficient in recording of PA signals and has generally resulted in reduced image quality and lack of quantification abilities, mainly because of the limited tomographic view of the linear-array geometry (53). Recent approaches for efficient hybridization consist ofadapting concave array geometry typically used in small-animal MSOT systems (133, 207) for concurrent photoacoustic-ultrasound imaging (208, 209). Due to their larger angular tomographic coverage, hand-held MSOT scanners based on concave arrays outperform those based on linear arrays in terms of signal quantification abilities and overall image quality (210). Most recently, a multi-segment detector array approach incorporating array segments of linear and concave geometry to optimally support both ultrasound and optoacoustic image acquisition has been introduced (211). The new approach enabled the acquisition of high-quality anatomical data by both modalities complemented by functional information on blood oxygenation status provided by MSOT (212).

4. Representative Applications of PAT in Life Sciences and Clinical Studies

The advances in PAT have enabled numerous applications in life science and clinical studies that are not attainable by current technologies. In this section, we highlight several representative applications to demonstrate PAT's potential impact, while many other exciting works cannot be covered due to the page limit. In Table 1, we have summarized representative PAT applications over a wide range of scales. Readers are strongly referred to other comprehensive reviews on PAT's latest applications. Overall, from single cell analysis to intraoperative imaging guidance, PAT has been applied in a broad range of fundamental studies, and the translation of PAT from lab technology to clinical impact is accelerating.

4.1. PAT Applications in Life Sciences

For fundamental research, PAT can visualize tissue functions with molecular specificity, on the single vessel, single cell, or even subcellular levels (43). Quantitative analysis of the photoacoustic signals acquired from single vessels/cells can provide information about their anatomical, mechanical, functional, and molecular properties, which can be used to enhance the understanding of biological processes at the microscopic level. It is important to note that the label-free imaging capability of PAT is often highly desirable in biomedical studies in order to improve the throughput and mitigate the labeling artifacts. For example, Wang *et al.* have used high-resolution high-speed PAM to track the oxygen release from single red blood cells flowing in capillaries in a mouse brain (258). Moreover, a recent work has demonstrated label-free histology-like assessment of tumor margins in human lumpectomy specimen, taking advantage of PAM's intrinsic sensitivity to DNA and RNA within the ultraviolet wavelength range (259). This work has also been expanded to image the whole organs *ex vivo* by microtomy-assisted PAM (260).

4.2. PAT on the Move to Clinical Studies

For human studies, PAT has been increasingly utilized for cancer detection (199, 200), surgery guidance (201–204), and treatment monitoring (205–207). Early-stage breast cancer detection is one of the major applications of PAT moving quickly towards clinical translation, taking advantage of PAT's high sensitivity to tumor hypoxia and angiogenesis. To this end, several groups have reported promising clinical studies on breast cancer patients. For example, the Twente PA mammography, illustrated in Fig. 5(a), has recently demonstrated the detection of 31 malignant breast tumors, with a sensitivity of 96.8% (208). The LOUISA-3D system can provide volumetric human breast vasculature, clearly showing the tumor structure (209). MSOT has also been applied in human breast imaging, providing tumor visualization with recurring features such as high-peripheral low-intratumoral vascularity, and increased total blood volume heterogeneity (261). Another direction of clinical study using PAT is dermatology. For example, Chuah *et al.* have developed volumetric MSOT (vMSOT) to image skin cancers with good correlation with histology results, demonstrating universally high accuracy regardless of the tumor types and skin conditions (262). In another study of dermatology, dual-mode PAT/OCT was able to identify skins with different types of dermatitis, such as chronic hyperkeratotic hand eczema, chronic hand eczema, and atopic dermatitis inflammatory skin disease (Fig. 5(c)) (263). PAT has also been applied in oral health and otorhinolaryngology. One example is the portable OR-PAM of early-stage oral cancer, which depicts the vascular networks in the human lips up to 0.5 mm in depth (Fig. 5(b)) (264). In another study by Zhao *et al.* (265), PAT was used for detecting thyroid cancer together with color Doppler ultrasound (Fig. 5(d)), in which PAT provided detailed information of the tumor vasculature at a depth of 2 cm on patients with suspicious malignant thyroid nodules (265). More recently, Ivankovic *et al.* (266) demonstrated a hand-held vMSOT system for real-time volumetric imaging of the human carotid artery with a 2-cm^3 field-of-view (Fig. 5(f)). This system opens up a wide range of applications in cardiovascular diseases, especially in early assessment of stroke risk. MSOT has also been utilized in assessing Crohn's diseases by evaluating hemoglobin signals in the intestinal walls (Fig. 5(e)) (267), and metastasis status of sentinel lymph nodes (SLN) in melanoma by using indocyanine green (ICG) as the contrast agent (Fig. 5(g)) (268). Besides the above human studies, several other PAT technologies are on the horizon of clinical translations (269, 270). For instance, transrectal PAT is under development for prostate cancer detection and biopsy guidance (59, 244). PAT-enhanced robotic surgical system is promising for guiding endonasal and fetal surgery with high precision (247, 248, 250, 271). Temperature mapping is another focus of PAT's treatment guidance, especially for HIFU ablation and interstitial laser phototherapy (136, 253, 254, 272).

5. Conclusions and Future Prospects of PAT

In this concise Review article, we have introduced recent advances in PAT technologies, as well as their representative applications in life sciences and clinical studies. As a fast developing technology, PAT has a great potential to enable novel biomedical discoveries and generate significant clinical impact. PAT is a highly scalable imaging modality providing balanced spatial resolution over a wide range of penetration depth. Its functional and molecular sensitivity originates from the unique optical absorption contrast, and has enabled

the measurements of a large number of physiological parameters. Enabled by multi-spectral signal analysis, PAT can image numerous endogenous and exogenous contrast agents, with high molecular specificity.

5.1. Technical challenges of PAT

Despite its powerful imaging performance and exciting new applications, PAT still has several major challenges remained to be addressed. First of all, the limited penetration is PAT's most significant drawback when compared with other whole-body imaging modalities. At present, PAT has reached up to 5 cm using external light illumination (262), which is insufficient for many clinical applications such as kidney and liver imaging. Secondly, wavelength-dependent light attenuation in living tissues leads to unknown local optical fluence at depths, preventing accurate quantitative imaging. Thirdly, super-resolution PAM has made significant progress in the recent years, but its low signal-to-noise ratio still prevents single-molecular imaging. Fourth, due to the strong acoustic aberrations introduced by air cavities and bones (273), PAT has difficulties in imaging the lungs and brain (274), especially for human applications (275). Last but not least, image artifacts due to sub-optimal data acquisition (e.g. limited-view or limited-detection-bandwidth) often lead to reduced imaging quality.

5.2. Potential Future Prospects of PAT

The above challenges have also pointed out the potential future prospects of PAT. A number of technological breakthroughs are anticipated in the coming years. Currently, super-resolution PAM, discussed in Section 3.3.1, has achieved approximately 100 nm spatial resolution with various nonlinear signal generation mechanisms. Future development of SR-PAM using higher-order nonlinearity will achieve even better resolutions on the level of ~50 nm, and may provide single molecule sensitivity. Such a high resolution and sensitivity will enable PAM to compete with other super-resolution imaging modalities such as photo-activated localization microscopy and stimulated emission depletion microscopy (276). Secondly, PAT is highly promising for functional brain imaging of direct neural activities in small animal models, using NIR voltage- or calcium-sensitive indicators that are specially engineered for enhanced optical absorbance. PAT possesses intrinsic advantages over conventional optical microscopy in terms of penetration depth. The current voltage- and calcium-sensitive indicators are mostly designed for fluorescent imaging in the visible wavelength range, and thus not ideal for PAT's deep-penetrating applications. Recent advances in protein engineering have shown great promise for developing NIR protein sensors (277), whereas the first NIR calcium-sensitive protein has been recently reported (278). Thirdly, multi-scale multi-parameter PAT as a single imaging device is possible. As discussed above, existing PAT systems have been individually applied for measuring functional and molecular information at different scales, ranging from organelles to organs. Future developments in PAT may integrate different imaging scales into one device and can measure multiple parameters simultaneously. Doing this, PAT's multi-scale multi-contrast imaging capability can be truly realized, enabling the studies of the same biological process at different scales. Lastly, low-cost compact PAT systems may become highly beneficial for longitudinal monitoring of physiological parameters such as oxygenation, blood flow, and glucose level. They may also find use in detecting circulating tumor cells as an independent

assessment of cancer metastatic potential and evaluation of treatment efficacy, such as immunotherapy and chemotherapy (279, 280). With the initial success on low-cost PAT using laser diodes, further advances in compressed sensing and machine learning can reduce the hardware complexity and overall system costs.

Acknowledgements

We acknowledge the support from National Institute of Health grants R01 EB028143, R01 NS111039, and R21 EB027304, Duke MEDx Basic Science Pilot Grant, Duke Center for Genomic and Computational Biology Faculty Pilot Research Grant; American Heart Association Collaborative Sciences Award (18CSA34080277) (all to J.Y.). Financial support is also acknowledged from the European Research Council Grant ERC-2015-CoG-682379, National Institute of Health grants R21 EY028365 and UF1 NS107680, Human Frontier Science Program Grant RGY0070/2016, and German research Foundation Grant RA1848/5–1 (all to D.R.).

References

1. Lee S-Y, Lai Y-H, Huang K-C, Cheng Y-H, Tseng T-F, Sun C-K. In vivo sub-femtoliter resolution photoacoustic microscopy with higher frame rates. Scientific reports. 2015;5:15421. [PubMed: 26487363]
2. Danielli A, Maslov KI, Garcia-Uribe A, Winkler AM, Li C, Wang L, et al. Label-free photoacoustic nanoscopy. Journal of biomedical optics. 2014;19(8):086006. [PubMed: 25104412]
3. Wang L, Zhang C, Wang LV. Grueneisen relaxation photoacoustic microscopy. Physical review letters. 2014;113(17):174301. [PubMed: 25379919]
4. Bell AG. Upon the production and reproduction of sound by light. Journal of the Society of Telegraph Engineers. 1880;9(34):404–26.
5. Landa FJO, Deán-Ben XL, Sroka R, Razansky D. Volumetric optoacoustic temperature mapping in photothermal therapy. Scientific reports. 2017;7(1):9695. [PubMed: 28851968]
6. Yao J, Kaberniuk AA, Li L, Shcherbakova DM, Zhang R, Wang L, et al. Multiscale photoacoustic tomography using reversibly switchable bacterial phytochrome as a near-infrared photochromic probe. Nature methods. 2016;13(1):67. [PubMed: 26550774]
7. Yao J, Wang L, Li C, Zhang C, Wang LV. Photoimprint photoacoustic microscopy for three-dimensional label-free subdiffraction imaging. Physical review letters. 2014;112(1):014302. [PubMed: 24483902]
8. Bardsley P, Ren K, Zhang R. Quantitative photoacoustic imaging of two-photon absorption. Journal of biomedical optics. 2018;23(1):016002.
9. Ren K, Zhang R. Nonlinear quantitative photoacoustic tomography with two-photon absorption. SIAM Journal on Applied Mathematics. 2018;78(1):479–503.
10. Yamaoka Y, Kimura Y, Harada Y, Takamatsu T, Takahashi E, editors. Fast focus-scanning head in two-photon photoacoustic microscopy with electrically-controlled liquid lens Photons Plus Ultrasound: Imaging and Sensing 2018; 2018: International Society for Optics and Photonics.
11. Danielli A, Maslov K, Favazza CP, Xia J, Wang LV. Nonlinear photoacoustic spectroscopy of hemoglobin. Applied physics letters. 2015;106(20):203701. [PubMed: 26045627]
12. Deán-Ben X, Razansky D. Optoacoustic signal excitation with a tone-burst of short pulses. Photoacoustics. 2018;11:1. [PubMed: 30003040]
13. Li M, Tang Y, Yao J. Photoacoustic Tomography of Blood Oxygenation: A Mini Review. Photoacoustics. 2018.
14. Wang LV, Yao J. A practical guide to photoacoustic tomography in the life sciences. Nature methods. 2016;13(8):627. [PubMed: 27467726]
15. Yao J, Wang L, Yang J-M, Maslov KI, Wong TT, Li L, et al. High-speed label-free functional photoacoustic microscopy of mouse brain in action. Nature methods. 2015;12(5):407. [PubMed: 25822799]
16. Gao F, Feng X, Zhang R, Liu S, Ding R, Kishor R, et al. Single laser pulse generates dual photoacoustic signals for differential contrast photoacoustic imaging. Scientific Reports. 2017;7(1):626. [PubMed: 28377616]

17. Wang L, Xia J, Yao J, Maslov KI, Wang LV. Ultrasonically encoded photoacoustic flowgraphy in biological tissue. Physical review letters. 2013;111(20):204301. [PubMed: 24289689]
18. Gao L, Wang L, Li C, Garcia-Uribe A, Wang LV. Photothermal bleaching in time-lapse photoacoustic microscopy. Journal of biophotonics. 2013;6(6–7):543–8. [PubMed: 23184422]
19. Sarimollaoglu M, Nedosekin DA, Menyaev YA, Juratli MA, Zharov VP. Nonlinear photoacoustic signal amplification from single targets in absorption background. Photoacoustics. 2014;2(1):1–11. [PubMed: 24921062]
20. Galanzha EI, Nedosekin DA, Sarimollaoglu M, Orza AI, Biris AS, Verkhusha VV, et al. Photoacoustic and photothermal cytometry using photoswitchable proteins and nanoparticles with ultrasharp resonances. Journal of biophotonics. 2015;8(1–2):81–93. [PubMed: 24259123]
21. Vetschera P, Mishra k, Fuenzalida Werner J-P, Chmyrov A, Ntziachristos V, Stiel AC. Characterization of reversibly switchable fluorescent proteins (rsFPs) in optoacoustic imaging. Analytical chemistry. 2018.
22. Hauptmann A, Lucka F, Betcke M, Huynh N, Adler J, Cox B, et al. Model-Based Learning for Accelerated, Limited-View 3-D Photoacoustic Tomography. IEEE transactions on medical imaging. 2018;37(6):1382–93. [PubMed: 29870367]
23. Wang D, Wang Y, Wang W, Luo D, Chitgupi U, Geng J, et al. Deep tissue photoacoustic computed tomography with a fast and compact laser system. Biomedical optics express. 2017;8(1):112–23. [PubMed: 28101405]
24. Lucka F, Huynh NT, Betcke M, Zhang E, Beard P, Arridge S, et al., editors. Compressed sensing techniques for fast high-resolution 3D photoacoustic tomography (Conference Presentation) Photons Plus Ultrasound: Imaging and Sensing 2018; 2018: International Society for Optics and Photonics.
25. Ermolayev V, Dean-Ben XL, Mandal S, Ntziachristos V, Razansky D. Simultaneous visualization of tumour oxygenation, neovascularization and contrast agent perfusion by real-time three-dimensional optoacoustic tomography. European radiology. 2016;26(6):1843–51. [PubMed: 26334513]
26. Taruttis A, Ntziachristos V. Advances in real-time multispectral optoacoustic imaging and its applications. Nature Photonics. 2015;9(4):219.
27. Xia J, Wang LV. Small-animal whole-body photoacoustic tomography: a review. IEEE Trans Biomed Engineering. 2014;61(5):1380–9.
28. Jeon M, Kim J, Kim C. Multiplane spectroscopic whole-body photoacoustic imaging of small animals in vivo. Medical & biological engineering & computing. 2016;54(2–3):283–94. [PubMed: 25115270]
29. Vogt WC, Zhou X, Andriani R, Wear KA, Garra BS, Pfefer J, editors. Performance evaluation of photoacoustic oximetry imaging systems using a dynamic blood flow phantom with tunable oxygen saturation Photons Plus Ultrasound: Imaging and Sensing 2018; 2018: International Society for Optics and Photonics.
30. Zharov VP. Devices and methods for fractionated photoacoustic flow cytometry. Google Patents; 2018.
31. Nedosekin DA, Nolan J, Cai C, Bourdo SE, Nima Z, Biris AS, et al. In vivo noninvasive analysis of graphene nanomaterial pharmacokinetics using photoacoustic flow cytometry. Journal of Applied Toxicology. 2017;37(11):1297–304. [PubMed: 28524252]
32. Talukdar Y Carbon Nanoparticle Enhance Photoacoustic Imaging and Therapy for Bone Tissue Engineering: The Graduate School, Stony Brook University: Stony Brook, NY; 2017.
33. Ho J, Ogunlande O, Butler C, Janes S, Birchall M, Beard P, editors. In vivo monitoring of vascularisation of decellularised scaffolds in tissue engineering using photoacoustic tomography 2017: Annual Meeting of the Society-of-Academic-and-Research-Surgery (SARS).
34. Kang J, Zhang HK, Kadam SD, Fedorko J, Valentine H, Malla AP, et al. Transcranial in vivo recording of neural activity in the rodent brain with near-infrared photoacoustic voltage-sensitive dye imaging. bioRxiv. 2018:202408.
35. Arthuis CJ, Novell A, Raes F, Escoffre J-M, Lerondel S, Le Pape A, et al. Real-time monitoring of placental oxygenation during maternal hypoxia and hyperoxygenation using photoacoustic imaging. PloS one. 2017;12(1):e0169850. [PubMed: 28081216]

36. Hysi E, Wirtzfeld LA, Al-Mahrouki A, Law N, Elfarnawany M, Lacefield JC, et al., editors. Implications of tumor oxygenation and blood flow for cancer treatment monitoring using photoacoustic imaging and power Doppler Ultrasonics Symposium (IUS), 2017 IEEE International; 2017: IEEE.
37. Al Mukaddim R, Rodgers A, Hacker TA, Heinmiller A, Varghese T. Real-Time in Vivo Photoacoustic Imaging in the Assessment of Myocardial Dynamics in Murine Model of Myocardial Ischemia. Ultrasound in medicine & biology. 2018.
38. Diot G, Metz S, Noske A, Liapis E, Schroeder B, Ovsepian SV, et al. Multi-Spectral Optoacoustic Tomography (MSOT) of human breast cancer. Clinical Cancer Research. 2017:clincanres. 3200.2016.
39. Lin L, Hu P, Shi J, Appleton CM, Maslov K, Wang LV, editors. Clinical photoacoustic computed tomography of the human breast in vivo within a single breath hold Photons Plus Ultrasound: Imaging and Sensing 2018; 2018: International Society for Optics and Photonics.
40. Zhou Y, Tripathi SV, Rosman I, Ma J, Hai P, Linette GP, et al. Noninvasive determination of melanoma depth using a handheld photoacoustic probe. The Journal of investigative dermatology. 2017;137(6):1370. [PubMed: 28163070]
41. Zhou Y, Li G, Zhu L, Li C, Cornelius LA, Wang LV. Handheld photoacoustic probe to detect both melanoma depth and volume at high speed in vivo. Journal of biophotonics. 2015;8(11–12):961–7. [PubMed: 25676898]
42. Yao J, Wang LV. Recent progress in photoacoustic molecular imaging. Current opinion in chemical biology. 2018;45:104–12. [PubMed: 29631120]
43. Strohm EM, Moore MJ, Kolios MC. Single cell photoacoustic microscopy: a review. IEEE Journal of Selected Topics in Quantum Electronics. 2016;22(3):137–51.
44. van den Berg P, Daoudi K, Steenbergen W. Review of photoacoustic flow imaging: its current state and its promises. Photoacoustics. 2015;3(3):89–99. [PubMed: 26640771]
45. Brunker J, Yao J, Laufer J, Bohndiek SE. Photoacoustic imaging using genetically encoded reporters: a review. Journal of biomedical optics. 2017;22(7):070901.
46. Wu D, Huang L, Jiang MS, Jiang H. Contrast agents for photoacoustic and thermoacoustic imaging: a review. International journal of molecular sciences. 2014;15(12):23616–39. [PubMed: 25530615]
47. Weber J, Beard PC, Bohndiek SE. Contrast agents for molecular photoacoustic imaging. Nature methods. 2016;13(8):639. [PubMed: 27467727]
48. Patimisco P, Scamarcio G, Tittel FK, Spagnolo V. Quartz-enhanced photoacoustic spectroscopy: a review. Sensors. 2014;14(4):6165–206. [PubMed: 24686729]
49. Patimisco P, Sampaolo A, Zheng H, Dong L, Tittel FK, Spagnolo V. Quartz–enhanced photoacoustic spectrophones exploiting custom tuning forks: a review. Advances in Physics: X. 2017;2(1):169–87.
50. Upputuri PK, Pramanik M. Recent advances toward preclinical and clinical translation of photoacoustic tomography: a review. Journal of Biomedical Optics. 2016;22(4):041006.
51. Wang LV, Hu S. Photoacoustic tomography: in vivo imaging from organelles to organs. science. 2012;335(6075):1458–62. [PubMed: 22442475]
52. Beard P Biomedical photoacoustic imaging. Interface focus. 2011:rsfs20110028.
53. Lutzweiler C, Razansky D. Optoacoustic imaging and tomography: reconstruction approaches and outstanding challenges in image performance and quantification. Sensors. 2013;13(6):7345–84. [PubMed: 23736854]
54. Moore MJ, Schygulla PM, Strohm EM, Kolios MC, editors. Single red blood cell oxygenation saturation imaging with multispectral photoacoustic microscopy Ultrasonics Symposium (IUS), 2016 IEEE International; 2016: IEEE.
55. Zhang YS, Yao J, Zhang C, Li L, Wang LV, Xia Y. Optical-Resolution Photoacoustic Microscopy for Volumetric and Spectral Analysis of Histological and Immunochemical Samples. Angewandte Chemie. 2014;126(31):8237–41.
56. Strohm EM, Moore MJ, Kolios MC. High resolution ultrasound and photoacoustic imaging of single cells. Photoacoustics. 2016;4(1):36–42. [PubMed: 27114911]

57. Zhang HF, Maslov K, Stoica G, Wang LV. Functional photoacoustic microscopy for high-resolution and noninvasive in vivo imaging. Nature biotechnology. 2006;24(7):848.
58. Yao J, Wang LV. Photoacoustic brain imaging: from microscopic to macroscopic scales. Neurophotonics. 2014;1(1):011003.
59. Li M, Lan B, Liu W, Xia J, Yao J. Internal-illumination photoacoustic computed tomography. Journal of biomedical optics. 2018;23(3):030506.
60. Lin L, Xia J, Wong TT, Li L, Wang LV. In vivo deep brain imaging of rats using oral-cavity illuminated photoacoustic computed tomography. Journal of biomedical optics. 2015;20(1): 016019. [PubMed: 25611865]
61. Deán-Ben X, Gottschalk S, Mc Larney B, Shoham S, Razansky D. Advanced optoacoustic methods for multiscale imaging of in vivo dynamics. Chemical Society Reviews. 2017;46(8): 2158–98. [PubMed: 28276544]
62. Hennen SN, Xing W, Shui Y-B, Zhou Y, Kalishman J, Andrews-Kaminsky LB, et al. Photoacoustic tomography imaging and estimation of oxygen saturation of hemoglobin in ocular tissue of rabbits. Experimental eye research. 2015;138:153–8. [PubMed: 26048477]
63. Zhang HF, Maslov K, Sivaramakrishnan M, Stoica G, Wang LV. Imaging of hemoglobin oxygen saturation variations in single vessels in vivo using photoacoustic microscopy. Applied physics letters. 2007;90(5):053901.
64. Wang Y, Hu S, Maslov K, Zhang Y, Xia Y, Wang LV. In vivo integrated photoacoustic and confocal microscopy of hemoglobin oxygen saturation and oxygen partial pressure. Optics letters. 2011;36(7):1029–31. [PubMed: 21478972]
65. Zhang L, Sheng D, Wang D, Yao Y, Yang K, Wang Z, et al. Bioinspired Multifunctional Melanin-Based Nanoliposome for Photoacoustic/Magnetic Resonance Imaging-Guided Efficient Photothermal Ablation of Cancer. Theranostics. 2018;8(6):1591. [PubMed: 29556343]
66. Sethuraman S, Amirian JH, Litovsky SH, Smalling RW, Emelianov SY. Ex vivo characterization of atherosclerosis using intravascular photoacoustic imaging. Optics express. 2007;15(25):16657–66. [PubMed: 19550952]
67. Jansen K, Van Der Steen AF, van Beusekom HM, Oosterhuis JW, van Soest G. Intravascular photoacoustic imaging of human coronary atherosclerosis. Optics letters. 2011;36(5):597–9. [PubMed: 21368919]
68. Luke GP, Yeager D, Emelianov SY. Biomedical applications of photoacoustic imaging with exogenous contrast agents. Ann Biomed Eng. 2012;40(2):422–37. [PubMed: 22048668]
69. Kim C, Favazza C, Wang LHV. In Vivo Photoacoustic Tomography of Chemicals: High-Resolution Functional and Molecular Optical Imaging at New Depths. Chem Rev. 2010;110(5):2756–82. [PubMed: 20210338]
70. Jokerst JV, Van de Sompel D, Bohndiek SE, Gambhir SS. Cellulose nanoparticles are a biodegradable photoacoustic contrast agent for use in living mice. Photoacoustics. 2014;2(3):119–27. [PubMed: 25225633]
71. Jokerst JV, Bohndiek SE, Gambhir SS, editors. Cellulose nanoparticles: Photoacoustic contrast agents that biodegrade to simple sugars Photons Plus Ultrasound: Imaging and Sensing 2014; 2014: International Society for Optics and Photonics.
72. Chen Q, Liu X, Chen J, Zeng J, Cheng Z, Liu Z. A self-assembled albumin-based nanoprobe for in vivo ratiometric photoacoustic pH imaging. Advanced Materials. 2015;27(43):6820–7. [PubMed: 26418312]
73. Chen Q, Liu X, Zeng J, Cheng Z, Liu Z. Albumin-NIR dye self-assembled nanoparticles for photoacoustic pH imaging and pH-responsive photothermal therapy effective for large tumors. Biomaterials. 2016;98:23–30. [PubMed: 27177219]
74. Cheng X, Sun R, Yin L, Chai Z, Shi H, Gao M. Light-Triggered Assembly of Gold Nanoparticles for Photothermal Therapy and Photoacoustic Imaging of Tumors In Vivo. Advanced Materials. 2017;29(6):1604894.
75. Sun I-C, Dumani D, Emelianov SY, editors. Ultrasound-guided photoacoustic imaging of lymph nodes with biocompatible gold nanoparticles as a novel contrast agent (Conference Presentation) Colloidal Nanoparticles for Biomedical Applications XII; 2017: International Society for Optics and Photonics.

76. Li W, Chen X. Gold nanoparticles for photoacoustic imaging. Nanomedicine. 2015;10(2):299–320. [PubMed: 25600972]
77. Li K, Liu B. Polymer-encapsulated organic nanoparticles for fluorescence and photoacoustic imaging. Chemical Society Reviews. 2014;43(18):6570–97. [PubMed: 24792930]
78. Pu K, Mei J, Jokerst JV, Hong G, Antaris AL, Chattopadhyay N, et al. Diketopyrrolopyrrole-based semiconducting polymer nanoparticles for in vivo photoacoustic imaging. Advanced Materials. 2015;27(35):5184–90. [PubMed: 26247171]
79. Huynh E, Leung BY, Helfield BL, Shakiba M, Gandier J-A, Jin CS, et al. In situ conversion of porphyrin microbubbles to nanoparticles for multimodality imaging. Nature nanotechnology. 2015;10(4):325.
80. Huynh E, Lovell JF, Helfield BL, Jeon M, Kim C, Goertz DE, et al. Porphyrin shell microbubbles with intrinsic ultrasound and photoacoustic properties. Journal of the American Chemical Society. 2012;134(40):16464–7. [PubMed: 22827774]
81. Kim C, Qin R, Xu JS, Wang LV, Xu RX. Multifunctional microbubbles and nanobubbles for photoacoustic and ultrasound imaging. Journal of biomedical optics. 2010;15(1):010510. [PubMed: 20210423]
82. Zipfel WR, Williams RM, Webb WW. Nonlinear magic: multiphoton microscopy in the biosciences. Nature biotechnology. 2003;21(11):1369.
83. Denk W, Strickler JH, Webb WW. Two-photon laser scanning fluorescence microscopy. Science. 1990;248(4951):73–6. [PubMed: 2321027]
84. Yamaoka Y, Harada Y, Sakakura M, Minamikawa T, Nishino S, Maehara S, et al. Photoacoustic microscopy using ultrashort pulses with two different pulse durations. Optics express. 2014;22(14):17063–72. [PubMed: 25090520]
85. Yamaoka Y, Nambu M, Takamatsu T, editors. Frequency-selective multiphoton-excitation-induced photoacoustic microscopy (MEPAM) to visualize the cross sections of dense objects Photons Plus Ultrasound: Imaging and Sensing 2010; 2010: International Society for Optics and Photonics.
86. Yamaoka Y, Nambu M, Takamatsu T. Fine depth resolution of two-photon absorption-induced photoacoustic microscopy using low-frequency bandpass filtering. Optics express. 2011;19(14): 13365–77. [PubMed: 21747492]
87. Yamaoka Y, Harada Y, Nishino S, Maehara S, Hamano S, Takamatsu T, editors. Improvement of signal detection selectivity and efficiency in two-photon absorption-induced photoacoustic microscopy Photons Plus Ultrasound: Imaging and Sensing 2014; 2014: International Society for Optics and Photonics.
88. Shelton RL, Applegate BE. Ultrahigh resolution photoacoustic microscopy via transient absorption. Biomedical optics express. 2010;1(2):676–86. [PubMed: 21258499]
89. Mattison SP, Mondragon E, Kaunas R, Applegate BE. Hybrid nonlinear photoacoustic and reflectance confocal microscopy for label-free subcellular imaging with a single light source. Optics letters. 2017;42(19):4028–31. [PubMed: 28957189]
90. Shi J, Wang L, Noordam C, Wang LV. Bessel-beam Grueneisen relaxation photoacoustic microscopy with extended depth of field. Journal of biomedical optics. 2015;20(11):116002. [PubMed: 26524679]
91. Yao J, Wang L, Li C, Zhang C, Wang LV, editors. Photo-imprint super-resolution photoacoustic microscopy Photons Plus Ultrasound: Imaging and Sensing 2015; 2015: International Society for Optics and Photonics.
92. Nedosekin DA, Galanzha EI, Dervishi E, Biris AS, Zharov VP. Super-resolution nonlinear photothermal microscopy. Small. 2014;10(1):135–42. [PubMed: 23864531]
93. Stiel AC, Deán-Ben XL, Jiang Y, Ntziachristos V, Razansky D, Westmeyer GG. High-contrast imaging of reversibly switchable fluorescent proteins via temporally unmixed multispectral optoacoustic tomography. Optics letters. 2015;40(3):367–70. [PubMed: 25680049]
94. Chaigne T, Arnal B, Vilov S, Bossy E, Katz O. Super-resolution photoacoustic imaging via flow-induced absorption fluctuations. Optica. 2017;4(11):1397–404.
95. Chaigne T, Gateau J, Allain M, Katz O, Gigan S, Sentenac A, et al. Super-resolution photoacoustic fluctuation imaging with multiple speckle illumination. Optica. 2016;3(1):54–7.

96. Conkey DB, Caravaca-Aguirre AM, Dove JD, Ju H, Murray TW, Piestun R. Super-resolution photoacoustic imaging through a scattering wall. Nature communications. 2015;6:7902.

97. Dean-Ben XL, Razansky D. Localization optoacoustic tomography. Light: Science & Applications. 2018;7(4):18004.

98. Deán-Ben XL, Fehm TF, Gostic M, Razansky D. Volumetric hand-held optoacoustic angiography as a tool for real-time screening of dense breast. Journal of biophotonics. 2016;9(3):253–9. [PubMed: 25966021]

99. Deán-Ben XL, Ozbek A, Razansky D. Volumetric real-time tracking of peripheral human vasculature with GPU-accelerated three-dimensional optoacoustic tomography. IEEE transactions on medical imaging. 2013;32(11):2050–5. [PubMed: 23846468]

100. Gottschalk S, Fehm TF, Deán-Ben XL, Tsytsarev V, Razansky D. Correlation between volumetric oxygenation responses and electrophysiology identifies deep thalamocortical activity during epileptic seizures. Neurophotonics. 2016;4(1):011007. [PubMed: 27725948]

101. Donoho DL. Compressed sensing. IEEE Transactions on information theory. 2006;52(4):1289–306.

102. Meng J, Wang LV, Ying L, Liang D, Song L. Compressed-sensing photoacoustic computed tomography in vivo with partially known support. Optics Express. 2012;20(15):16510–23.

103. Cao M, Yuan J, Du S, Xu G, Wang X, Carson PL, et al. Full-view photoacoustic tomography using asymmetric distributed sensors optimized with compressed sensing method. Biomedical Signal Processing and Control. 2015;21:19–25.

104. Haltmeier M, Berer T, Moon S, Burgholzer P. Compressed sensing and sparsity in photoacoustic tomography. Journal of Optics. 2016;18(11):114004.

105. Arridge S, Beard P, Betcke M, Cox B, Huynh N, Lucka F, et al. Accelerated high-resolution photoacoustic tomography via compressed sensing. Physics in Medicine & Biology. 2016;61(24):8908. [PubMed: 27910824]

106. Sandbichler M, Krahmer F, Berer T, Burgholzer P, Haltmeier M. A novel compressed sensing scheme for photoacoustic tomography. SIAM Journal on Applied Mathematics. 2015;75(6):2475–94.

107. Özbek A, Deán-Ben XL, Razansky D. Optoacoustic imaging at kilohertz volumetric frame rates. Optica. 2018;5(7):857–63. [PubMed: 31608306]

108. Meng J, Jiang Z, Wang LV, Park J, Kim C, Sun M, et al. High-speed, sparse-sampling three-dimensional photoacoustic computed tomography in vivo based on principal component analysis. Journal of biomedical optics. 2016;21(7):076007.

109. Nagaoka R, Yamazaki R, Saijo Y. Adaptive Spatial Filtering with Principal Component Analysis for Biomedical Photoacoustic Imaging. Physics Procedia. 2015;70:1161–4.

110. Song K, Wang LV. Deep reflection-mode photoacoustic imaging of biological tissue. Journal of biomedical optics. 2007;12(6):060503. [PubMed: 18163798]

111. Xia J, Chatni MR, Maslov KI, Guo Z, Wang K, Anastasio MA, et al. Whole-body ring-shaped confocal photoacoustic computed tomography of small animals in vivo. Journal of biomedical optics. 2012;17(5):050506. [PubMed: 22612121]

112. Razansky D, Buehler A, Ntziachristos V. Volumetric real-time multispectral optoacoustic tomography of biomarkers. Nature protocols. 2011;6(8):1121. [PubMed: 21738125]

113. Xia J, Chen W, Maslov KI, Anastasio MA, Wang LV. Retrospective respiration-gated whole-body photoacoustic computed tomography of mice. Journal of biomedical optics. 2014;19(1):016003.

114. Li L, Zhu L, Ma C, Lin L, Yao J, Wang L, et al., editors. Imaging small animal whole-body dynamics by single-impulse panoramic photoacoustic computed tomography Photons Plus Ultrasound: Imaging and Sensing 2017; 2017: International Society for Optics and Photonics.

115. Li L, Zhu L, Ma C, Lin L, Yao J, Wang L, et al. Single-impulse panoramic photoacoustic computed tomography of small-animal whole-body dynamics at high spatiotemporal resolution. Nature biomedical engineering. 2017;1(5):0071.

116. Liba O, de la Zerda A. Photoacoustic tomography: Breathtaking whole-body imaging. Nature Biomedical Engineering. 2017;1(5):0075.

117. Merčep E, Herraiz JL, Deán-Ben XL, Razansky D. Transmission–reflection optoacoustic ultrasound (TROPUS) computed tomography of small animals. Light: Science & Applications. 2019;8(1):18.
118. Fehm TF, Deán-Ben XL, Ford SJ, Razansky D. In vivo whole-body optoacoustic scanner with real-time volumetric imaging capacity. Optica. 2016;3(11):1153–9.
119. Deán-Ben XL, Fehm TF, Ford SJ, Gottschalk S, Razansky D. Spiral volumetric optoacoustic tomography visualizes multi-scale dynamics in mice. Light: Science & Applications. 2017;6(4):e16247.
120. Wissmeyer G, Pleitez MA, Rosenthal A, Ntziachristos V. Looking at sound: optoacoustics with all-optical ultrasound detection. Light: Science & Applications. 2018;7(1):53.
121. Ogunlade O, Connell JJ, Huang JL, Zhang E, Lythgoe MF, Long DA, et al. In vivo 3-dimensional photoacoustic imaging of the renal vasculature in preclinical rodent models. American Journal of Physiology-Renal Physiology. 2017.
122. Plumb AA, Huynh NT, Guggenheim J, Zhang E, Beard P. Rapid volumetric photoacoustic tomographic imaging with a Fabry-Perot ultrasound sensor depicts peripheral arteries and microvascular vasomotor responses to thermal stimuli. European radiology. 2018;28(3):1037–45. [PubMed: 29018924]
123. Huynh N, Ogunlade O, Zhang E, Cox B, Beard P, editors. Photoacoustic imaging using an 8-beam Fabry-Perot scanner Photons Plus Ultrasound: Imaging and Sensing 2016; 2016: International Society for Optics and Photonics.
124. Huynh N, Lucka F, Zhang E, Betcke M, Arridge S, Beard P, et al., editors. Sub-sampled Fabry-Perot photoacoustic scanner for fast 3D imaging Photons Plus Ultrasound: Imaging and Sensing 2017; 2017: International Society for Optics and Photonics.
125. Guggenheim JA, Li J, Allen TJ, Colchester RJ, Noimark S, Ogunlade O, et al. Ultrasensitive plano-concave optical microresonators for ultrasound sensing. Nature Photonics. 2017;11(11): 714.
126. Wang Y, Wang D, Hubbell R, Xia J. Second generation slit-based photoacoustic tomography system for vascular imaging in human. Journal of biophotonics. 2017;10(6–7):799–804. [PubMed: 27935228]
127. Wang Y, Wang D, Zhang Y, Geng J, Lovell JF, Xia J. Slit-enabled linear-array photoacoustic tomography with near isotropic spatial resolution in three dimensions. Optics letters. 2016;41(1): 127–30. [PubMed: 26696175]
128. Dai X, Yang H, Jiang H. In vivo photoacoustic imaging of vasculature with a low-cost miniature light emitting diode excitation. Optics letters. 2017;42(7):1456–9. [PubMed: 28362791]
129. Hansen RS, editor Using high-power light emitting diodes for photoacoustic imaging. Medical Imaging 2011: Ultrasonic Imaging, Tomography, and Therapy; 2011: International Society for Optics and Photonics.
130. Dai X, Yang H, Jiang H, editors. Low-cost high-power light emitting diodes for photoacoustic imaging Photons Plus Ultrasound: Imaging and Sensing 2017; 2017: International Society for Optics and Photonics.
131. Upputuri PK, Pramanik M. Performance characterization of low-cost, high-speed, portable pulsed laser diode photoacoustic tomography (PLD-PAT) system. Biomedical optics express. 2015;6(10):4118–29. [PubMed: 26504659]
132. Daoudi K, Van Den Berg P, Rabot O, Kohl A, Tisserand S, Brands P, et al. Handheld probe integrating laser diode and ultrasound transducer array for ultrasound/photoacoustic dual modality imaging. Optics express. 2014;22(21):26365–74. [PubMed: 25401669]
133. Buehler A, Kacprowicz M, Taruttis A, Ntziachristos V. Real-time handheld multispectral optoacoustic imaging. Optics letters. 2013;38(9):1404–6. [PubMed: 23632499]
134. Herzog E, Taruttis A, Beziere N, Lutich AA, Razansky D, Ntziachristos V. Optical imaging of cancer heterogeneity with multispectral optoacoustic tomography. Radiology. 2012;263(2):461–8. [PubMed: 22517960]
135. Wang L, Li G, Xia J, Wang LV. Ultrasonic-heating-encoded photoacoustic tomography with virtually augmented detection view. Optica. 2015;2(4):307–12. [PubMed: 25984555]

136. Wang L, Yao J, Maslov KI, Xing W, Wang LV. Ultrasound-heated photoacoustic flowmetry. Journal of biomedical optics. 2013;18(11):117003. [PubMed: 24194064]

137. Zhang R, Wang L, Yao J, Yeh C-H, Wang LV. In vivo optically encoded photoacoustic flowgraphy. Optics letters. 2014;39(13):3814–7. [PubMed: 24978744]

138. Liu W, Lan B, Hu L, Chen R, Zhou Q, Yao J. Photoacoustic thermal flowmetry with a single light source. Journal of biomedical optics. 2017;22(9):096001.

139. Shao Q, Ashkenazi S. Photoacoustic lifetime imaging for direct in vivo tissue oxygen monitoring. Journal of biomedical optics. 2015;20(3):036004. [PubMed: 25748857]

140. Morgounova E, Shao Q, Hackel BJ, Thomas DD, Ashkenazi S. Photoacoustic lifetime contrast between methylene blue monomers and self-quenched dimers as a model for dual-labeled activatable probes. Journal of biomedical optics. 2013;18(5):056004.

141. Shao Q, Morgounova E, Choi J-H, Jiang C, Bischof J, Ashkenazi S, editors. Mapping tissue oxygen in vivo by photoacoustic lifetime imaging Photons Plus Ultrasound: Imaging and Sensing 2013; 2013: International Society for Optics and Photonics.

142. Shao Q, Morgounova E, Ashkenazi S, editors. Tissue oxygen monitoring by photoacoustic lifetime imaging (PALI) and its application to image-guided photodynamic therapy (PDT) Photons Plus Ultrasound: Imaging and Sensing 2015; 2015: International Society for Optics and Photonics.

143. Tzoumas S, Ntziachristos V. Spectral unmixing techniques for optoacoustic imaging of tissue pathophysiology. Philosophical Transactions of the Royal Society A: Mathematical, Physical and Engineering Sciences. 2017;375(2107):20170262.

144. Tzoumas S, Nunes A, Olefir I, Stangl S, Symvoulidis P, Glasl S, et al. Eigenspectra optoacoustic tomography achieves quantitative blood oxygenation imaging deep in tissues. Nature communications. 2016;7:ncomms12121.

145. Namita T, Sato M, Kondo K, Yamakawa M, Shiina T, editors. Evaluation of blood glucose concentration measurement using photoacoustic spectroscopy in near-infrared region Photons Plus Ultrasound: Imaging and Sensing 2017; 2017: International Society for Optics and Photonics.

146. Sim JY, Ahn C-G, Jeong E-J, Kim BK. In vivo Microscopic Photoacoustic Spectroscopy for Non-Invasive Glucose Monitoring Invulnerable to Skin Secretion Products. Scientific reports. 2018;8(1):1059. [PubMed: 29348411]

147. Pai PP, Sanki PK, Banerjee S, editors. A photoacoustics based continuous non-invasive blood glucose monitoring system MeMeA; 2015.

148. Pai PP, Sanki PK, Sarangi S, Banerjee S. Modelling, verification, and calibration of a photoacoustics based continuous non-invasive blood glucose monitoring system. Review of Scientific Instruments. 2015;86(6):064901. [PubMed: 26133859]

149. Tachibana K, Okada K, Kobayashi R, Ishihara Y, editors. Development of a high-sensitivity and portable cell using Helmholtz resonance for noninvasive blood glucose-level measurement based on photoacoustic spectroscopy Engineering in Medicine and Biology Society (EMBC), 2016 IEEE 38th Annual International Conference of the; 2016: IEEE.

150. Tajima T, Tanaka Y, Nakamura M, Seyama M, editors. Multi-modality analysis of glucose aqueous solution using photoacoustic and dielectric spectroscopy for non-invasive glucose monitoring Photons Plus Ultrasound: Imaging and Sensing 2017; 2017: International Society for Optics and Photonics.

151. Gao L, Wang L, Li C, Liu Y, Ke H, Zhang C, et al. Single-cell photoacoustic thermometry. Journal of biomedical optics. 2013;18(2):026003.

152. Pramanik M, Wang LV. Thermoacoustic and photoacoustic sensing of temperature. Journal of biomedical optics. 2009;14(5):054024. [PubMed: 19895126]

153. Ke H, Tai S, Wang LV. Photoacoustic thermography of tissue. Journal of biomedical optics. 2014;19(2):026003. [PubMed: 24522803]

154. Liu S, Feng X, Ruochong Z, Zheng Y, editors. Portable photoacoustic system for noninvasive blood temperature measurement Circuits and Systems (ISCAS), 2018 IEEE International Symposium on; 2018: IEEE.

155. Liao Y, Jian X, Dong F, Cui Y, editors. Dual-wavelengths photoacoustic temperature measurement. Second International Conference on Photonics and Optical Engineering; 2017: International Society for Optics and Photonics.

156. Yao J, Ke H, Tai S, Zhou Y, Wang LV. Absolute photoacoustic thermometry in deep tissue. Optics letters. 2013;38(24):5228–31. [PubMed: 24322224]

157. Zhou Y, Tang E, Luo J, Yao J. Deep-tissue temperature mapping by multi-illumination photoacoustic tomography aided by a diffusion optical model: a numerical study. J Biomed Opt. 2018;23(1):1–10.

158. Alaeian M, Orlande HRB, Lamien B. Application of the photoacoustic technique for temperature measurements during hyperthermia. Inverse Problems in Science and Engineering. 2018:1–21.

159. Pu K, Shuhendler AJ, Jokerst JV, Mei J, Gambhir SS, Bao Z, et al. Semiconducting polymer nanoparticles as photoacoustic molecular imaging probes in living mice. Nature nanotechnology. 2014;9(3):233.

160. Miao Q, Pu K. Emerging designs of activatable photoacoustic probes for molecular imaging. Bioconjugate chemistry. 2016;27(12):2808–23. [PubMed: 27998078]

161. Miao Q, Lyu Y, Ding D, Pu K. Semiconducting oligomer nanoparticles as an activatable photoacoustic probe with amplified brightness for in vivo imaging of pH. Advanced Materials. 2016;28(19):3662–8. [PubMed: 27000431]

162. Zhou EY, Knox HJ, Reinhardt CJ, Partipilo G, Nilges MJ, Chan J. Near-Infrared Photoactivatable Nitric Oxide Donors with Integrated Photoacoustic Monitoring. Journal of the American Chemical Society. 2018.

163. Ding K, Zeng J, Jing L, Qiao R, Liu C, Jiao M, et al. Aqueous synthesis of PEGylated copper sulfide nanoparticles for photoacoustic imaging of tumors. Nanoscale. 2015;7(25):11075–81. [PubMed: 26055816]

164. Chen F, Hong H, Goel S, Graves SA, Orbay H, Ehlerding EB, et al. In vivo tumor vasculature targeting of CuS@ MSN based theranostic nanomedicine. ACS nano. 2015;9(4):3926–34. [PubMed: 25843647]

165. Zhou M, Li J, Liang S, Sood AK, Liang D, Li C. CuS nanodots with ultrahigh efficient renal clearance for positron emission tomography imaging and image-guided photothermal therapy. ACS nano. 2015;9(7):7085–96. [PubMed: 26098195]

166. Wang G, Zhang F, Tian R, Zhang L, Fu G, Yang L, et al. Nanotubes-embedded indocyanine green–hyaluronic acid nanoparticles for photoacoustic-imaging-guided phototherapy. ACS applied materials & interfaces. 2016;8(8):5608–17. [PubMed: 26860184]

167. Zhang L, Gao S, Zhang F, Yang K, Ma Q, Zhu L. Activatable hyaluronic acid nanoparticle as a theranostic agent for optical/photoacoustic image-guided photothermal therapy. Acs Nano. 2014;8(12):12250–8. [PubMed: 25402600]

168. Xie C, Upputuri PK, Zhen X, Pramanik M, Pu K. Self-quenched semiconducting polymer nanoparticles for amplified in vivo photoacoustic imaging. Biomaterials. 2017;119:1–8. [PubMed: 27988405]

169. Lyu Y, Fang Y, Miao Q, Zhen X, Ding D, Pu K. Intraparticle molecular orbital engineering of semiconducting polymer nanoparticles as amplified theranostics for in vivo photoacoustic imaging and photothermal therapy. ACS nano. 2016;10(4):4472–81. [PubMed: 26959505]

170. Xia J, Pelivanov IM, Wei C-W, Hu X, Gao X, O'Donnell M. Suppression of background signal in magnetomotive photoacoustic imaging of magnetic microspheres mimicking targeted cells. Journal of biomedical optics. 2012;17(6):061224. [PubMed: 22734754]

171. Jia C, Xia J, Pelivanov IM, Seo CH, Hu X, Jin Y, et al., editors. Dynamic manipulation of magnetic contrast agents in photoacoustic imaging Photons Plus Ultrasound: Imaging and Sensing 2011; 2011: International Society for Optics and Photonics.

172. Li J, Arnal B, Wei C-W, Shang J, Nguyen T-M, O'Donnell M, et al. Magneto-optical nanoparticles for cyclic magnetomotive photoacoustic imaging. ACS nano. 2015;9(2):1964–76. [PubMed: 25658655]

173. Dana N, Fowler R, Allen A, Zoldan J, Suggs L, Emelianov S. In vitro photoacoustic sensing of calcium dynamics with arsenazo III. Laser Physics Letters. 2016;13(7):075603.

174. Deán-Ben XL, Sela G, Lauri A, Kneipp M, Ntziachristos V, Westmeyer GG, et al. Functional optoacoustic neuro-tomography for scalable whole-brain monitoring of calcium indicators. Light: Science & Applications. 2016;5(12):e16201.
175. Roberts S, Seeger M, Jiang Y, Mishra A, Sigmund F, Stelzl A, et al. Calcium sensor for photoacoustic imaging. Journal of the American Chemical Society. 2017;140(8):2718–21. [PubMed: 28945084]
176. Mishra A, Jiang Y, Roberts S, Ntziachristos V, Westmeyer GG. Near-infrared photoacoustic imaging probe responsive to calcium. Analytical chemistry. 2016;88(22):10785–9. [PubMed: 27779396]
177. Li H, Zhang P, Smaga LP, Hoffman RA, Chan J. Photoacoustic probes for ratiometric imaging of copper (II). Journal of the American Chemical Society. 2015;137(50):15628–31. [PubMed: 26652006]
178. Zhang D, Wu M, Zeng Y, Liao N, Cai Z, Liu G, et al. Lipid micelles packaged with semiconducting polymer dots as simultaneous MRI/photoacoustic imaging and photodynamic/photothermal dual-modal therapeutic agents for liver cancer. Journal of Materials Chemistry B. 2016;4(4):589–99.
179. Liang X, Li Y, Li X, Jing L, Deng Z, Yue X, et al. PEGylated Polypyrrole Nanoparticles Conjugating Gadolinium Chelates for Dual-Modal MRI/Photoacoustic Imaging Guided Photothermal Therapy of Cancer. Advanced Functional Materials. 2015;25(9):1451–62.
180. Qin H, Zhou T, Yang S, Chen Q, Xing D. Gadolinium (III)-gold nanorods for MRI and photoacoustic imaging dual-modality detection of macrophages in atherosclerotic inflammation. Nanomedicine. 2013;8(10):1611–24. [PubMed: 23351094]
181. Kircher MF, De La Zerda A, Jokerst JV, Zavaleta CL, Kempen PJ, Mittra E, et al. A brain tumor molecular imaging strategy using a new triple-modality MRI-photoacoustic-Raman nanoparticle. Nature medicine. 2012;18(5):829.
182. Qin C, Cheng K, Chen K, Hu X, Liu Y, Lan X, et al. Tyrosinase as a multifunctional reporter gene for Photoacoustic/MRI/PET triple modality molecular imaging. Scientific reports. 2013;3:1490. [PubMed: 23508226]
183. Tian C, Feng T, Wang C, Liu S, Cheng Q, Oliver DE, et al. Non-contact photoacoustic imaging using a commercial heterodyne interferometer. IEEE sensors journal. 2016;16(23):8381–8. [PubMed: 28210188]
184. Rousseau G, Blouin A, Monchalin J-P. Non-contact photoacoustic tomography and ultrasonography for tissue imaging. Biomedical optics express. 2012;3(1):16–25. [PubMed: 22254164]
185. Jathoul AP, Laufer J, Ogunlade O, Treeby B, Cox B, Zhang E, et al. Deep in vivo photoacoustic imaging of mammalian tissues using a tyrosinase-based genetic reporter. Nature Photonics. 2015;9(4):239.
186. Wang Y, Li C, Wang RK. Noncontact photoacoustic imaging achieved by using a low-coherence interferometer as the acoustic detector. Optics letters. 2011;36(20):3975–7. [PubMed: 22002357]
187. Berer T, Hochreiner A, Zamiri S, Burgholzer P. Remote photoacoustic imaging on solid material using a two-wave mixing interferometer. Optics letters. 2010;35(24):4151–3. [PubMed: 21165120]
188. Hochreiner A, Berer T, Grün H, Leitner M, Burgholzer P. Photoacoustic imaging using an adaptive interferometer with a photorefractive crystal. Journal of biophotonics. 2012;5(7):508–17. [PubMed: 22354686]
189. Buj C, Horstmann J, Münter M, Brinkmann R. Speckle-based holographic detection for non-contact Photoacoustic Tomography. Proc Biomed Tech. 2014;59:844.
190. Horstmann J, Spahr H, Buj C, Münter M, Brinkmann R. Full-field speckle interferometry for non-contact photoacoustic tomography. Physics in Medicine & Biology. 2015;60(10):4045. [PubMed: 25927910]
191. Hochreiner A, Bauer-Marschallinger J, Burgholzer P, Jakoby B, Berer T. Non-contact photoacoustic imaging using a fiber based interferometer with optical amplification. Biomedical optics express. 2013;4(11):2322–31. [PubMed: 24298397]

192. Park SJ, Eom J, Kim YH, Lee CS, Lee BH. Noncontact photoacoustic imaging based on all-fiber heterodyne interferometer. Optics letters. 2014;39(16):4903–6. [PubMed: 25121904]

193. Hochreiner A, Bauer-Marschallinger J, Burgholzer P, Berer T, editors. Fiber-based remote photoacoustic imaging utilizing a Mach Zehnder interferometer with optical amplification Photons Plus Ultrasound: Imaging and Sensing 2014; 2014: International Society for Optics and Photonics.

194. Bauer-Marschallinger J, Felbermayer K, Berer T. All-optical photoacoustic projection imaging. Biomedical optics express. 2017;8(9):3938–51. [PubMed: 29026680]

195. Bauer-Marschallinger J, Felbermayer K, Bouchal K-D, Veres IA, Grün H, Burgholzer P, et al., editors. Photoacoustic projection imaging using a 64-channel fiber optic detector array Photons Plus Ultrasound: Imaging and Sensing 2015; 2015: International Society for Optics and Photonics.

196. Hajireza P, Shi W, Bell K, Paproski RJ, Zemp RJ. Non-interferometric photoacoustic remote sensing microscopy. Light: Science & Applications. 2017;6(6):e16278.

197. Waibel D, Gröhl J, Isensee F, Kirchner T, Maier-Hein K, Maier-Hein L, editors. Reconstruction of initial pressure from limited view photoacoustic images using deep learning Photons Plus Ultrasound: Imaging and Sensing 2018; 2018: International Society for Optics and Photonics.

198. Antholzer S, Haltmeier M, Schwab J. Deep learning for photoacoustic tomography from sparse data. Inverse Problems in Science and Engineering. 2018:1–19.

199. Allman D, Reiter A, Bell MAL, editors. A machine learning method to identify and remove reflection artifacts in photoacoustic channel data Ultrasonics Symposium (IUS), 2017 IEEE International; 2017: IEEE.

200. Reiter A, Bell MAL, editors. A machine learning approach to identifying point source locations in photoacoustic data Photons Plus Ultrasound: Imaging and Sensing 2017; 2017: International Society for Optics and Photonics.

201. Paltauf G, Hartmair P, Kovachev G, Nuster R. Piezoelectric line detector array for photoacoustic tomography. Photoacoustics. 2017;8:28–36. [PubMed: 28971019]

202. Schwab J, Antholzer S, Nuster R, Haltmeier M. Real-time photoacoustic projection imaging using deep learning. arXiv preprint arXiv:180106693. 2018.

203. Schwab J, Antholzer S, Nuster R, Haltmeier M. DALnet: High-resolution photoacoustic projection imaging using deep learning. arXiv preprint arXiv:180106693. 2018.

204. Kirchner T, Gröhl J, Maier-Hein L. Context encoding enables machine learning-based quantitative photoacoustics. arXiv preprint arXiv:170603595. 2017.

205. Cai C, Deng K, Ma C, Luo J. End-to-end deep neural network for optical inversion in quantitative photoacoustic imaging. Optics letters. 2018;43(12):2752–5. [PubMed: 29905680]

206. Niederhauser JJ, Jaeger M, Lemor R, Weber P, Frenz M. Combined ultrasound and optoacoustic system for real-time high-contrast vascular imaging in vivo. IEEE transactions on medical imaging. 2005;24(4):436–40. [PubMed: 15822801]

207. Dima A, Ntziachristos V. Non-invasive carotid imaging using optoacoustic tomography. Optics express. 2012;20(22):25044–57. [PubMed: 23187270]

208. Merčep E, Burton NC, Claussen J, Razansky D. Whole-body live mouse imaging by hybrid reflection-mode ultrasound and optoacoustic tomography. Optics letters. 2015;40(20):4643–6. [PubMed: 26469584]

209. Mercep E, Jeng G, Morscher S, Li P-C, Razansky D. Hybrid optoacoustic tomography and pulse-echo ultrasonography using concave arrays. IEEE transactions on ultrasonics, ferroelectrics, and frequency control. 2015;62(9):1651–61.

210. Schellenberg MW, Hunt HK. Hand-held optoacoustic imaging: A review. Photoacoustics. 2018.

211. Merčep E, Deán-Ben XL, Razansky D. Combined pulse-echo ultrasound and multispectral optoacoustic tomography with a multi-segment detector array. IEEE transactions on medical imaging. 2017;36(10):2129–37. [PubMed: 28541198]

212. Merčep E, Deán-Ben XL, Razansky D. Imaging of blood flow and oxygen state with a multi-segment optoacoustic ultrasound array. Photoacoustics. 2018;10:48–53. [PubMed: 29988801]

213. Strohm EM, Berndl ES, Kolios MC. Probing red blood cell morphology using high-frequency photoacoustics. Biophysical journal. 2013;105(1):59–67. [PubMed: 23823224]

214. Yao D-K, Maslov K, Shung KK, Zhou Q, Wang LV. In vivo label-free photoacoustic microscopy of cell nuclei by excitation of DNA and RNA. Optics letters. 2010;35(24):4139–41. [PubMed: 21165116]

215. Imai T, Shi J, Wong TT, Li L, Zhu L, Wang LV. High-throughput ultraviolet photoacoustic microscopy with multifocal excitation. Journal of biomedical optics. 2018;23(3):036007.

216. Liu X, Wong TT, Shi J, Ma J, Yang Q, Wang LV. Label-free cell nuclear imaging by Grüneisen relaxation photoacoustic microscopy. Optics letters. 2018;43(4):947–50. [PubMed: 29444034]

217. Wang C, Ma X, Ye S, Cheng L, Yang K, Guo L, et al. Protamine functionalized single-walled carbon nanotubes for stem cell labeling and in vivo raman/magnetic resonance/photoacoustic triple-modal imaging. Advanced Functional Materials. 2012;22(11):2363–75.

218. Donnelly EM, Kubelick KP, Dumani DS, Emelianov SY. Photoacoustic Image-Guided Delivery of Plasmonic-Nanoparticle-Labeled Mesenchymal Stem Cells to the Spinal Cord. Nano letters. 2018;18(10):6625–32. [PubMed: 30160124]

219. Qin X, Chen H, Yang H, Wu H, Zhao X, Wang H, et al. Photoacoustic Imaging of Embryonic Stem Cell-Derived Cardiomyocytes in Living Hearts with Ultrasensitive Semiconducting Polymer Nanoparticles. Advanced Functional Materials. 2018;28(1):1704939. [PubMed: 30473658]

220. Talukdar Y, Avti P, Sun J, Sitharaman B. Multimodal ultrasound-photoacoustic imaging of tissue engineering scaffolds and blood oxygen saturation in and around the scaffolds. Tissue Engineering Part C: Methods. 2014;20(5):440–9. [PubMed: 24107069]

221. Nasiriavanaki M, Xia J, Wan H, Bauer AQ, Culver JP, Wang LV, editors. Resting-state functional connectivity imaging of the mouse brain using photoacoustic tomography Photons Plus Ultrasound: Imaging and Sensing 2014; 2014: International Society for Optics and Photonics.

222. Hariri A, Bely N, Chen C, Nasiriavanaki M, editors. Towards ultrahigh resting-state functional connectivity in the mouse brain using photoacoustic microscopy Photons Plus Ultrasound: Imaging and Sensing 2016; 2016: International Society for Optics and Photonics.

223. Nasiriavanaki M, editor Resting-state functional connectivity measurement in the mouse brain using a low cost photoacoustic computed tomography Frontiers in Optics; 2016: Optical Society of America.

224. Nasiriavanaki M, Xia J, Wan H, Bauer AQ, Culver JP, Wang LV. High-resolution photoacoustic tomography of resting-state functional connectivity in the mouse brain. Proceedings of the National Academy of Sciences. 2014;111(1):21–6.

225. Cui L, Rao J. Semiconducting polymer nanoparticles as photoacoustic molecular imaging probes. Wiley Interdisciplinary Reviews: Nanomedicine and Nanobiotechnology. 2017;9(2):e1418.

226. Kang J, Chang JH, Kim SM, Lee HJ, Kim H, Wilson BC, et al. Real-time sentinel lymph node biopsy guidance using combined ultrasound, photoacoustic, fluorescence imaging: in vivo proof-of-principle and validation with nodal obstruction. Scientific Reports. 2017;7:45008. [PubMed: 28327582]

227. Cai C, Carey KA, Nedosekin DA, Menyaev YA, Sarimollaoglu M, Galanzha EI, et al. In vivo photoacoustic flow cytometry for early malaria diagnosis. Cytometry Part A. 2016;89(6):531–42.

228. Zhou Q, Yang P, Wang Q, Pang K, Zhou H, He H, et al., editors. Label-free counting of circulating cells by in vivo photoacoustic flow cytometry Biophotonics and Immune Responses XIII; 2018: International Society for Optics and Photonics.

229. Wang Q, Pang K, Zhou Q, Yang P, He H, Wei X, editors. Improving label-free detection of circulating melanoma cells by photoacoustic flow cytometry Biophotonics and Immune Responses XIII; 2018: International Society for Optics and Photonics.

230. Juratli MA, Sarimollaoglu M, Siegel ER, Nedosekin DA, Galanzha EI, Suen JY, et al. Real-time monitoring of circulating tumor cell release during tumor manipulation using in vivo photoacoustic and fluorescent flow cytometry. Head & neck. 2014;36(8):1207–15. [PubMed: 23913663]

231. Yang P, Liu R, Niu Z, Suo Y, He H, Wei X, editors. Noninvasive and label-free detection of circulating melanoma cells by in vivo photoacoustic flow cytometry Biophotonics and Immune Responses X; 2015: International Society for Optics and Photonics.

232. Fakhrejahani E, Torii M, Kitai T, Kanao S, Asao Y, Hashizume Y, et al. Clinical report on the first prototype of a photoacoustic tomography system with dual illumination for breast cancer imaging. PloS one. 2015;10(10):e0139113. [PubMed: 26506106]

233. Heijblom M, Steenbergen W, Manohar S. Clinical photoacoustic breast imaging: the twente experience. IEEE pulse. 2015;6(3):42–6.

234. Heijblom M, Piras D, Xia W, van Hespen JC, Klaase J, Van den Engh F, et al. Visualizing breast cancer using the Twente photoacoustic mammoscope: what do we learn from twelve new patient measurements? Optics express. 2012;20(11):11582–97. [PubMed: 22714144]

235. Kitai T, Torii M, Sugie T, Kanao S, Mikami Y, Shiina T, et al. Photoacoustic mammography: initial clinical results. Breast Cancer. 2014;21(2):146–53. [PubMed: 22484692]

236. Garcia-Uribe A, Erpelding TN, Krumholz A, Ke H, Maslov K, Appleton C, et al. Dual-modality photoacoustic and ultrasound imaging system for noninvasive sentinel lymph node detection in patients with breast cancer. Scientific reports. 2015;5:15748. [PubMed: 26510774]

237. Xi L, Grobmyer SR, Zhou G, Qian W, Yang L, Jiang H. Molecular photoacoustic tomography of breast cancer using receptor targeted magnetic iron oxide nanoparticles as contrast agents. Journal of biophotonics. 2014;7(6):401–9. [PubMed: 23125139]

238. Oraevsky A, Su R, Nguyen H, Moore J, Lou Y, Bhadra S, et al., editors. Full-view 3D imaging system for functional and anatomical screening of the breast Photons Plus Ultrasound: Imaging and Sensing 2018; 2018: International Society for Optics and Photonics.

239. Klosner M, Chan G, Wu C, Heller DF, Su R, Ermilov S, et al., editors. Advanced laser system for 3D optoacoustic tomography of the breast Photons Plus Ultrasound: Imaging and Sensing 2016; 2016: International Society for Optics and Photonics.

240. Viator JA, Gupta S, Goldschmidt BS, Bhattacharyya K, Kannan R, Shukla R, et al. Gold nanoparticle mediated detection of prostate cancer cells using photoacoustic flowmetry with optical reflectance. Journal of biomedical nanotechnology. 2010;6(2):187–91. [PubMed: 20738074]

241. Su JL, Bouchard RR, Karpiouk AB, Hazle JD, Emelianov SY. Photoacoustic imaging of prostate brachytherapy seeds. Biomedical optics express. 2011;2(8):2243–54. [PubMed: 21833361]

242. Bell MAL, Kuo NP, Song DY, Kang JU, Boctor EM. In vivo visualization of prostate brachytherapy seeds with photoacoustic imaging. Journal of biomedical optics. 2014;19(12): 126011. [PubMed: 25531797]

243. Agarwal A, Huang S, O'donnell M, Day K, Day M, Kotov N, et al. Targeted gold nanorod contrast agent for prostate cancer detection by photoacoustic imaging. Journal of applied physics. 2007;102(6):064701.

244. Bell MAL, Guo X, Song DY, Boctor EM. Transurethral light delivery for prostate photoacoustic imaging. Journal of biomedical optics. 2015;20(3):036002. [PubMed: 25734406]

245. Piras D, Grijsen C, Schutte P, Steenbergen W, Manohar S. Photoacoustic needle: minimally invasive guidance to biopsy. Journal of biomedical optics. 2013;18(7):070502. [PubMed: 23817760]

246. Nguyen VP, Kim J, Ha K-l, Oh J, Kang HW. Feasibility study on photoacoustic guidance for high-intensity focused ultrasound-induced hemostasis. Journal of biomedical optics. 2014;19(10): 105010. [PubMed: 25354118]

247. Xia W, Maneas E, Nikitichev DI, Mosse CA, dos Santos GS, Vercauteren T, et al., editors. Interventional photoacoustic imaging of the human placenta with ultrasonic tracking for minimally invasive fetal surgeries International Conference on Medical Image Computing and Computer-Assisted Intervention; 2015: Springer.

248. Bell MAL, Dagle AB, Kazanzides P, Boctor EM, editors. Experimental assessment of energy requirements and tool tip visibility for photoacoustic-guided endonasal surgery Photons Plus Ultrasound: Imaging and Sensing 2016; 2016: International Society for Optics and Photonics.

249. Kim S, Tan Y, Kazanzides P, Bell MAL, editors. Feasibility of photoacoustic image guidance for telerobotic endonasal transsphenoidal surgery. Biomedical Robotics and Biomechatronics (BioRob), 2016 6th IEEE International Conference on; 2016: IEEE.

250. Eddins B, Bell MAL. Design of a multifiber light delivery system for photoacoustic-guided surgery. Journal of biomedical optics. 2017;22(4):041011.

251. Kim S, Kang HJ, Cheng A, Bell MAL, Boctor E, Kazanzides P, editors. Photoacoustic image guidance for robot-assisted skull base surgery. Robotics and Automation (ICRA), 2015 IEEE International Conference on; 2015: IEEE.
252. Gandhi N, Kim S, Kazanzides P, Bell MAL, editors. Accuracy of a novel photoacoustic-based approach to surgical guidance performed with and without a da Vinci robot Photons Plus Ultrasound: Imaging and Sensing 2017; 2017: International Society for Optics and Photonics.
253. Daoudi K, Hoogenboom M, den Brok M, Eikelenboom D, Adema GJ, Fütterer JJ, et al. In vivo photoacoustics and high frequency ultrasound imaging of mechanical high intensity focused ultrasound (HIFU) ablation. Biomedical optics express. 2017;8(4):2235–44. [PubMed: 28736668]
254. Dana N, Di Biase L, Natale A, Emelianov S, Bouchard R. In vitro photoacoustic visualization of myocardial ablation lesions. Heart Rhythm. 2014;11(1):150–7. [PubMed: 24080065]
255. Huang P, Lin J, Li W, Rong P, Wang Z, Wang S, et al. Biodegradable gold nanovesicles with an ultrastrong plasmonic coupling effect for photoacoustic imaging and photothermal therapy. Angewandte Chemie International Edition. 2013;52(52):13958–64. [PubMed: 24318645]
256. Liu Y, Bhattarai P, Dai Z, Chen X. Photothermal therapy and photoacoustic imaging via nanotheranostics in fighting cancer. Chemical Society Reviews. 2018.
257. Shah J, Park S, Aglyamov SR, Larson T, Ma L, Sokolov KV, et al. Photoacoustic imaging and temperature measurement for photothermal cancer therapy. Journal of biomedical optics. 2008;13(3):034024. [PubMed: 18601569]
258. Wang L, Maslov K, Wang LV. Single-cell label-free photoacoustic flowoxigraphy in vivo. Proc Natl Acad Sci U S A. 2013;110(15):5759–64. [PubMed: 23536296]
259. Wong TT, Zhang R, Hai P, Zhang C, Pleitez MA, Aft RL, et al. Fast label-free multilayered histology-like imaging of human breast cancer by photoacoustic microscopy. Science Advances. 2017;3(5):e1602168. [PubMed: 28560329]
260. Wong TT, Zhang R, Zhang C, Hsu H-C, Maslov KI, Wang L, et al. Label-free automated three-dimensional imaging of whole organs by microtomy-assisted photoacoustic microscopy. Nature communications. 2017;8(1):1386.
261. Diot G, Metz S, Noske A, Liapis E, Schroeder B, Ovsepian SV, et al. Multispectral optoacoustic tomography (MSOT) of human breast cancer. Clinical Cancer Research. 2017;23(22):6912–22. [PubMed: 28899968]
262. Chuah SY, Attia ABE, Ho CJH, Li X, Lee JS-S, Tan MWP, et al. Volumetric Multispectral Optoacoustic Tomography for 3-Dimensional Reconstruction of Skin Tumors: A Further Evaluation with Histopathologic Correlation. Journal of Investigative Dermatology. 2019;139(2): 481–5. [PubMed: 30227137]
263. Zabihian B, Weingast J, Liu M, Zhang E, Beard P, Pehamberger H, et al. In vivo dual-modality photoacoustic and optical coherence tomography imaging of human dermatological pathologies. Biomedical optics express. 2015;6(9):3163–78. [PubMed: 26417489]
264. Jin T, Guo H, Jiang H, Ke B, Xi L. Portable optical resolution photoacoustic microscopy (pORPAM) for human oral imaging. Optics letters. 2017;42(21):4434–7. [PubMed: 29088181]
265. Yang M, Zhao L, He X, Su N, Zhao C, Tang H, et al. Photoacoustic/ultrasound dual imaging of human thyroid cancers: an initial clinical study. Biomedical optics express. 2017;8(7):3449–57. [PubMed: 28717580]
266. Ivankovic I, Merčep E, Schmedt C-G, Deán-Ben XL, Razansky D. Real-time volumetric assessment of the human carotid artery: handheld multispectral optoacoustic tomography. Radiology. 2019:181325.
267. Knieling F, Neufert C, Hartmann A, Claussen J, Urich A, Egger C, et al. Multispectral optoacoustic tomography for assessment of Crohn's disease activity. New England Journal of Medicine. 2017;376(13):1292–4. [PubMed: 28355498]
268. Stoffels I, Morscher S, Helfrich I, Hillen U, Leyh J, Burton NC, et al. Metastatic status of sentinel lymph nodes in melanoma determined noninvasively with multispectral optoacoustic imaging. Science translational medicine. 2015;7(317):317ra199–317ra199.

269. Kim J, Park S, Jung Y, Chang S, Park J, Zhang Y, et al. Programmable real-time clinical photoacoustic and ultrasound imaging system. Scientific reports. 2016;6:35137. [PubMed: 27731357]

270. Valluru KS, Willmann JK. Clinical photoacoustic imaging of cancer. Ultrasonography. 2016;35(4):267. [PubMed: 27669961]

271. Kim S, Tan Y, Kazanzides P, Bell MAL, editors. Feasibility of photoacoustic image guidance for telerobotic endonasal transsphenoidal surgery. 2016 6th IEEE International Conference on Biomedical Robotics and Biomechatronics (BioRob); 2016: IEEE.

272. Li Z, Chen H, Zhou F, Li H, Chen W. Interstitial photoacoustic sensor for the measurement of tissue temperature during interstitial laser phototherapy. Sensors. 2015;15(3):5583–93. [PubMed: 25756865]

273. Deán-Ben XL, Ntziachristos V, Razansky D. Statistical optoacoustic image reconstruction using a-priori knowledge on the location of acoustic distortions. Applied Physics Letters. 2011;98(17): 171110.

274. Hc Estrada, Huang X, Rebling J, Zwack M, Gottschalk S, Razansky D. Virtual craniotomy for high-resolution optoacoustic brain microscopy. Scientific reports. 2018;8(1):1459. [PubMed: 29362486]

275. Estrada H, Gottschalk S, Reiss M, Neuschmelting V, Goldbrunner R, Razansky D. Observation of guided acoustic waves in a human skull. Ultrasound in medicine & biology. 2018;44(11):2388–92. [PubMed: 30093337]

276. Sydor AM, Czymmek KJ, Puchner EM, Mennella V. Super-resolution microscopy: from single molecules to supramolecular assemblies. Trends in cell biology. 2015;25(12):730–48. [PubMed: 26546293]

277. Chernov KG, Redchuk TA, Omelina ES, Verkhusha VV. Near-infrared fluorescent proteins, biosensors, and optogenetic tools engineered from phytochromes. Chemical reviews. 2017;117(9):6423–46. [PubMed: 28401765]

278. Qian Y, Piatkevich KD, Mc Larney B, Abdelfattah AS, Mehta S, Murdock MH, et al. A genetically encoded near-infrared fluorescent calcium ion indicator. Nature methods. 2019:1. [PubMed: 30573832]

279. Cristofanilli M, Budd GT, Ellis MJ, Stopeck A, Matera J, Miller MC, et al. Circulating tumor cells, disease progression, and survival in metastatic breast cancer. New England Journal of Medicine. 2004;351(8):781–91. [PubMed: 15317891]

280. Gupta GP, Massagué J. Cancer metastasis: building a framework. Cell. 2006;127(4):679–95. [PubMed: 17110329]

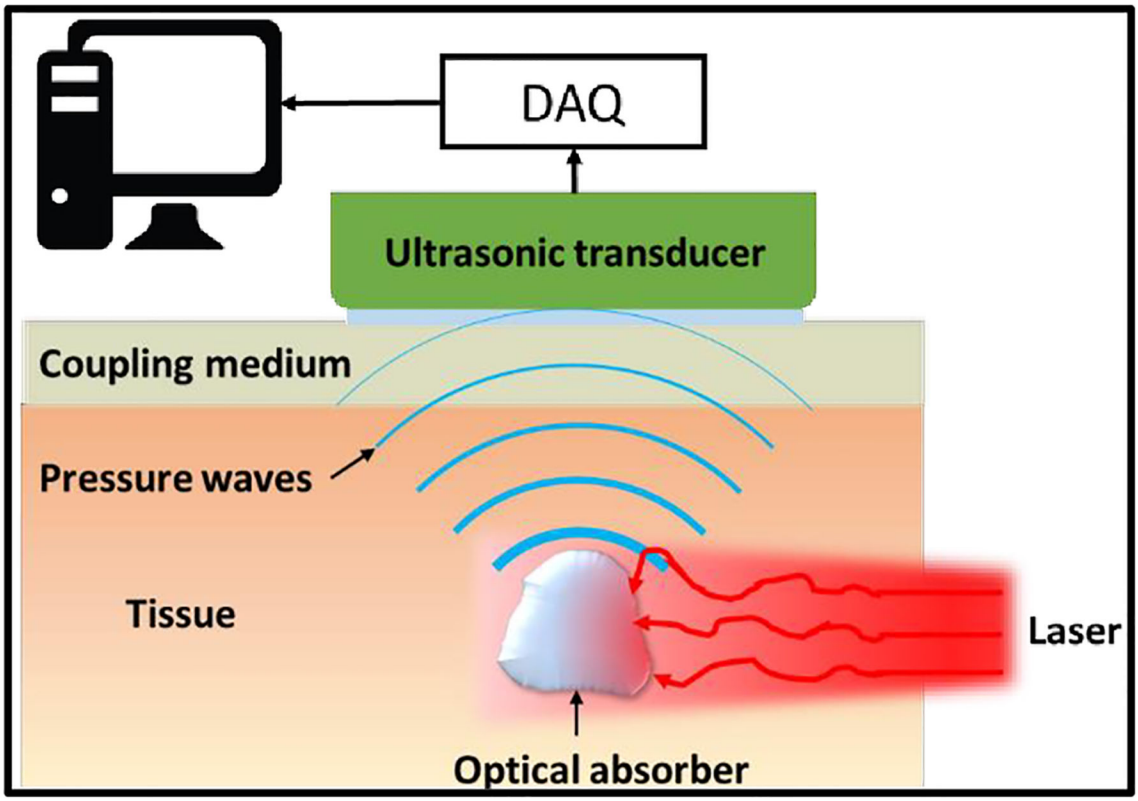

Figure 1.

Basic imaging scheme of PAT. Firstly, laser light is delivered to excite the target (optical absorber) in the tissue. The absorbed optical energy is partially or completely converted into heat, inducing a transient thermal expansion and local pressure rise. The pressure alterations propagate in tissues in the form of ultrasound waves, which are detected by ultrasonic detector(s) placed outside the tissue. After amplification and digitization, the detected signals are used to reconstruct the final PAT image reflecting optical absorption contrast inside tissues.

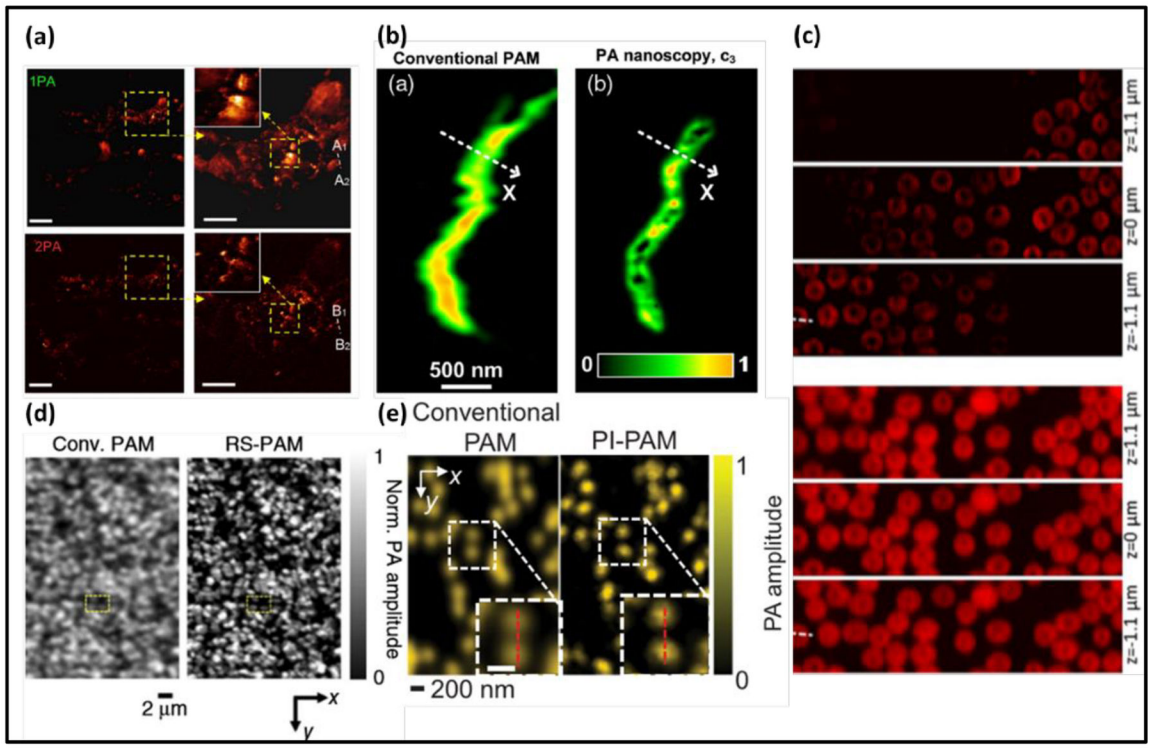

Figure 2.

Photoacoustic microscopy with sub-diffraction resolutions. (a) Melanin distribution imaged by two-photon PAM (2PA) (top) and one-photon PAM (1PA) (bottom) (1). (b) Mitochondria imaged by PA nanoscopy based on optical absorption saturation (2). (c) Red blood cells imaged by Grüneisen-relaxation-based PAM (GR-PAM) (top) at three different depths (3). (d) Reversibly-switchable PAM (RS-PAM) (right) has superior resolution on bacteria (left) (6). (e) Nanoparticles imaged by photobleaching-based PAM (PI-PAM) (right) (7).

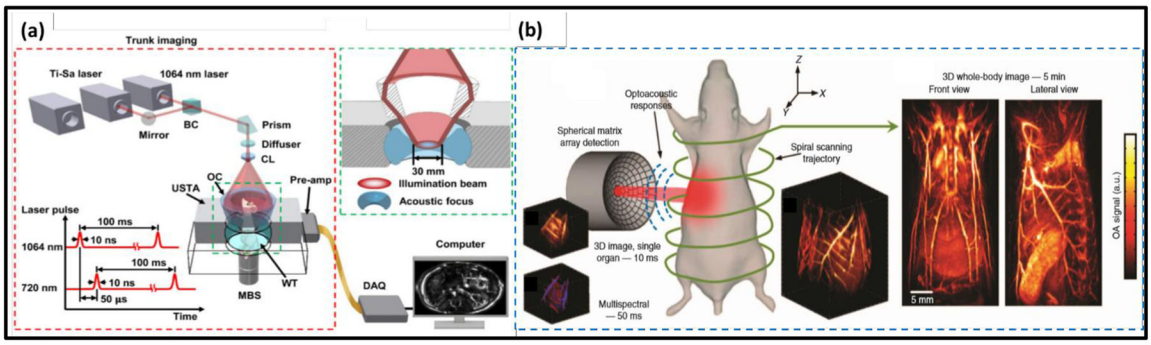

Figure 3.

Small-animal whole-body PACT. (a) Setup of the SIP-PACT system. A dual-wavelength illumination is employed for blood oxygenation estimation. BC: beam combiner; CL: conical lens; MBS: magnetic base scanner; OC: optical condenser; USTA: ultrasonic transducer array and WT: water tank (115). Each wavelength is illuminated at a 10-Hz pulse repetition rate. Adapted with permission from (115). (b) Setup of the SVOT system. The semi-spherical transducer array is rotated and translated along a spiral trajectory around the mouse to obtain consecutive volumetric images (left). Merging the individual volumes (middle) provides the final 3D whole-body image (right). Adapted with permissions from (119).

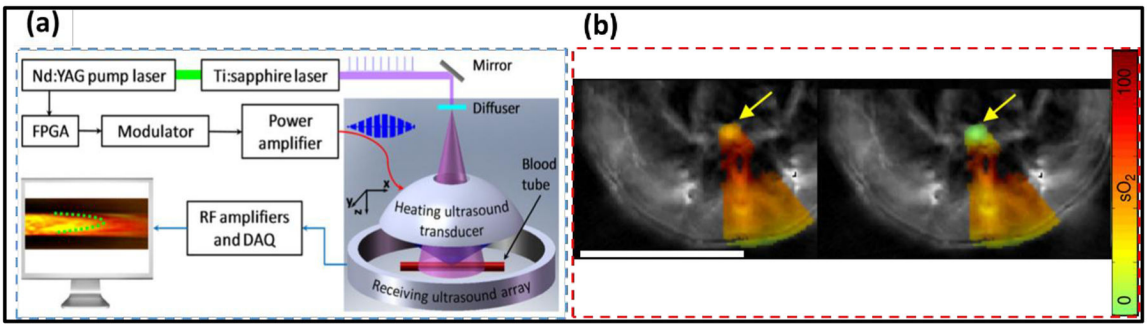

Figure 4.

Novel PAT methods for quantifying blood flow and oxygenation in deep tissues. (a) Imaging principle of UE-PAF. The ring-shaped ultrasound array tracks the displacement of HIFU-heated blood volume. Adapted with permission from (17). (b) Comparison of sO_2 quantification by using the traditional linear unmixing method (left) and eMSOT (right). The yellow arrows indicate a 0% sO_2 tube inserted inside the mouse tissue. Scale bar: 1 cm. Adapted with permission from (144).

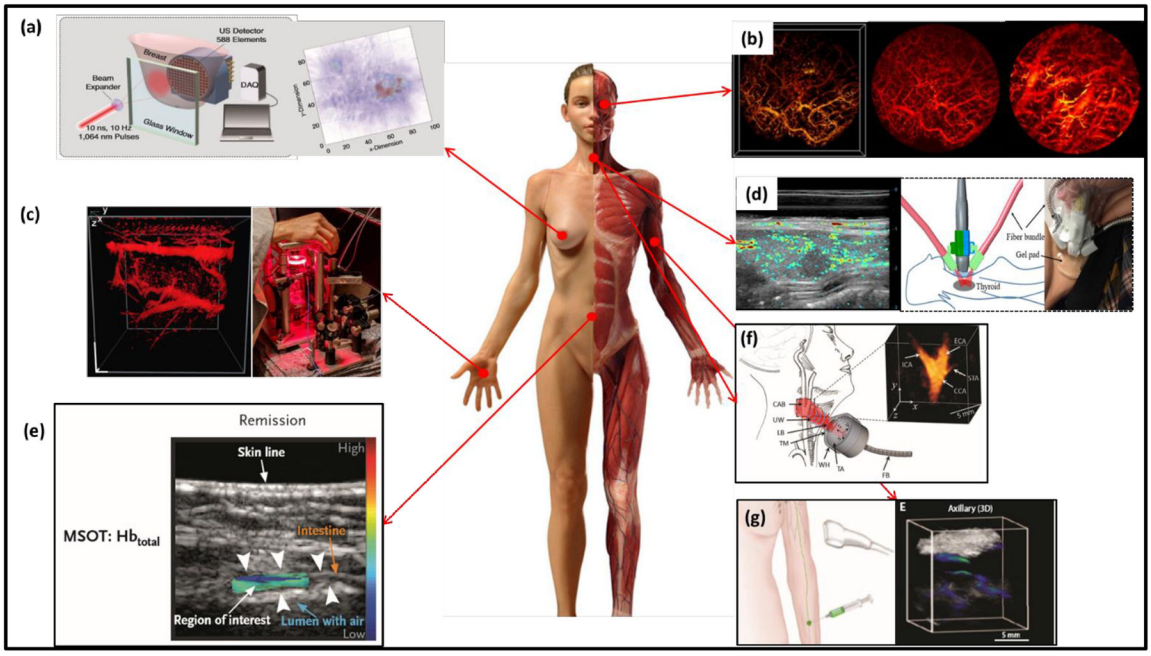

Figure 5.

Representative PAT applications on humans. (a) Twente photoacoustic mammoscopy for breast cancer imaging; left: overview of the system, right: MAP image of the breast showing the lesion clearly on the right side (233). (b) In vivo imaging of oral vasculature; left: 3D display of vessels in a human lip, middle: corresponding MAP image, and right: PA image of the deeper region (264). (c) In vivo imaging of the palm vessels; left: 3D image of the vascular network; right: the imaging system schematics (263). (d) Dual-mode PA/ultrasound imaging of human thyroid. Left: right lobe papillary thyroid cancer image. Right: schematics of the imaging system (265). (e) Illustration of the MSOT of inflammatory bowel disease (267). (f) vMSOT of the human carotid artery, showing the carotid bifurcation (266). (g) MSOT of SLN using ICG as the exogenous contrast (268).

Table 1.

Representative Applications of PAT

Applications	Imaging contrast/ principle	Measured information	PAT system	Selected ref
Cellular Imaging	Hemoglobin in red blood cells	RBC morphology, oxygen saturation, cell aggregation, stimulation-response	Ultra-high-frequency PAM	(54, 213, 214)
	DNA/RNA in cell nuclei	Cell nuclei morphology, nuclear size and packing density in tumor margin assessment	Ultraviolet (UV)-PAM	(214–216)
	Cytochrome in mitochondria	Mitochondria morphology and interconnectivity	OR-PAM/PA nanoscopy	(2, 151)
	Nanoparticle labeled stem cells	Track stem cell (embryonic, mesenchymal, etc.) migration	Dual-mode ultrasound-PACT	(217–219)
	Stained seed cells in engineered scaffolds	Track cell seeding within and quantify porosity and degradation of bio-scaffold	OR-/AR-PAM	(33, 167, 220)
Functional imaging	Oxy- and deoxy-hemoglobin	Map blood oxygenation of whole mouse cortex	MEMS OR-PAM	(15)
	Photoacoustic thermal tagging	Measure slow blood flow in deep mouse brain	PACT	(17, 136)
	Grüneisen parameter	Measure the tissue temperature during thermal therapy	PACT	(152, 153, 156)
	Hemodynamic fluctuation	Map brain's functional connectivity during resting state	PACT	(221–224)
Molecular imaging	Nanoparticle, organic dyes, genetically encoded chromophores	Use exogenous contrast agents as the probes for tumor imaging and cancer staging	PACT	(42, 225, 226)
Cancer imaging	Circulating tumor cells	Count the circulating tumor cells in melanoma as an independent indication of metastasis	PA flow cytometry	(227–231)
	Breast cancer	Estimate the breast tumor size based on the angiogenesis or labeled by nanoparticles	PA mammography	(232–239)
	Melanoma	Evaluate the volume, depth and thickness of melanoma and provide staging	PACT	(40, 41)
	Prostate cancer	Visualize prostate brachytherapy seeds, detect prostate cancer cells labelled by nanoparticles	PACT	(240–244)
Surgery or treatment guidance	Sentinel lymph node (SLN)	Track the needle tip and map SLN location during biopsy	PACT	(226, 245, 246)
	PA-guided surgery	Real-time guidance for endonasal surgery and minimally invasive fetal surgery	PACT integrated with surgical tools	(247–252)
	High-intensity focused ultrasound	Monitor temperature and blood oxygenation during HIFU ablation	PACT integrated with HIFU	(136, 253, 254)
	Photothermal therapy	Monitor the nanoparticle delivery during photothermal therapy	PACT	(255–257)